The People's Democratic Republic of Algeria

Ministry of Higher Education and Scientific Research

Amar Telidji University - Laghouat

Faculty of Sciences

Doctoral thesis

Specialty: material physics

Publicly presented on 18/12/2022
by:

Miss TOUIL Dalal Radia

THEME

Study, Design and Realization of GMR Probe for Eddy Current Non-Destructive Testing

Thesis committee:

Mr GUIBADJ Abdenacer	Professor	Amar Telidji Laghouat University	President
Mr BENSAID Samir	Professor	Akli Mohand Oulhadj Bouira University	Examiner
Mr CHERIET Ahmed	Professor	Mohamed Khider Biskra University	Examiner
Mr YOUSFI Belkacem	MCA	Amar Telidji Laghouat University	Examiner
Mr HELIFA Bachir	Professor	Amar Telidji Laghouat University	**Supervisor**
Mr LEFKAIER Iben Khaldoun	Professor	Amar Telidji Laghouat University	**Co-supervisor**

November 2022

Dedicate

To my dear mother
To my dear father's soul
To my dear grand mother
My big family
And all my friends

Acknowledgment

First, I thank ALLAH for giving me the faith and courage to complete this work. The present work is carried out in the Materials Physics Laboratory (LPM) of Laghouat University.

I want to express my deep gratitude to my supervisor **Mr. HELIFA Bachir,** a Professor at the University of Laghouat, who supervised me throughout this thesis and shared his brilliant ideas. Thanks for his kindness, constant availability, and encouragement.

I want to express my gratitude to my thesis co-supervisor, **Mr. Ibn Khaldoun LEFKAIER**, Chief of the Materials Physics Laboratory (LPM), a Professor at the University of Laghouat, and Thanks for his kindness, permanent availability, and encouragement.

Big thanks to **Mr. GUIBADJ Abdenacer**, Professor at Laghouat University, for the honor given to me to judge my thesis as a president.

I also thank **Mr. Samir BENSAID**, a Professor at Bouira University, for his participation in the jury of this thesis as an examiner.

I thank **Mr. CHERIET Ahmed**, a Professor at the University of Biskra, for agreeing to present on the jury as an examiner.

I thank **Mr. YOUSFI Belkacem**, MCA at the University of Laghouat, for the honor of judging my thesis as an examiner.

In addition, I express my gratitude to **Mr. DAAS Ahmed**, Prof-Assis B, for his precious help, valuable suggestions, and sound advice on how to carry out the work. Thank you, DAAS Ahmed.

I want to express my gratitude to **Mr. Ahmed Chaouki LAHRECH**, Prof-Assis B, for providing me with valuable suggestions, wise advice, and continued optimism and enthusiasm.Thank you Ahmed Chaouki LAHRECH.

Finally, thank all those who contributed directly or indirectly to the realization of my work.

Contents

Contents

CHAPTER 2 GMR PROBE DESIGN: SIMULATION IN EDDY CURRENT NON-DESTRUCTIVE TESTING (EC-NDT) SYSTEM

List of Tables

List of Tables

List of Figures

List of Figures

Abbreviations list

EC	Eddy Currents.
GMR	Giant Magnetoresistors.
ECT	Eddy Current Testing.
DAQ	Data Acquisition System.
ECP	Eddy Current Probe
FEM	Finite Element Method
NDE	Non-Destructive Evaluation
NDT	Non-Destructive Testing
EMF	Electromotive Force
ECNDT	Eddy Current Non-Destructive Testing
AMR	Anisotropic Magnetoresitors
SQUID	Superconducting Quantum Interference Device
TMR	Tunnel Magnetoresistance.

General Introduction

GENERAL INTRODUCTION

NDT is taken an increasingly important place in all high-tech industrial sectors. The economic stakes associated with NDT are still very high. In some industries, such as nuclear or transport, in particular aeronautics and maritime, they are coupled with a significant issue related to public safety.

Eddy Current Non-Destructive Testing (EC-NDT) is a reliable and sensitive method for detecting and measuring defects in a critical part. The determination of the parameters of a crack, for example, is still an open problem. The current challenge is to detect increasingly small defects while reducing inspection time.

EC-NDT methods have enhanced their effectiveness and efficiency through better sensor technologies, improved electronics and instrumentation, and robotic accessories. Advances in magnetic sensor technology are prompting researchers to investigate their capabilities on EC-NDTs. EC-NDT techniques can be fully explored with the emergence of these new sensors to detect small defects than before and characterize them geometrically [Postolache10].

The industry currently establishes several types of sensors used in EC-NDT. The most common eddy current probes are inductive sensors, fluxgates, magneto-impedances, Hall effect sensors, and magnetoresistance sensors.

Inductive sensors are most commonly used in EC-NDT. Their sensitivity in EC-NDT systems improves the detection performance of deep cracks [Hamia 13]. Nevertheless, low-frequency eddy currents (ECT) controls require sensors with high field sensitivity and spatial resolution [Hamia 10]. To exceed the performance of wire wound sensors in terms of sensitivity and resolution, we use giant magnetoresistance (GMR) [Rifai 16, Bernieri 19], characterized by high sensitivity at low frequency and wide dynamic range. We are relatively easy to perform and inexpensive [Zorni 12, Dogaru 01], which is suitable for many practical applications, including crack assessment [Rifai 16, Smith 04]. GMR sensors in the NDT field have triggered the development of very sensitive probes [Dogaru 01, Gao 18]. Nevertheless, GMR sensors for NDT applications are still under development; the development of magnetic sensors has made the use of low-frequency excitation fields possible and increased the method's sensitivity [Smith 99].

The objective of this thesis is to develop strategy of software and hardware tools for the design and construction of high-sensitivity magnetic sensors (GMR probe) in non-destructive testing by

eddy currents in its experimental and simulation for the characterization of cracks in "critical parts" of conductive materials.

We propose a novel design and implementation of a high-sensitivity GMR-based eddy current (EC) sensor to assess cracks in conductive materials. The originality of this approach uses two symmetrical Giant magnetoresistance sensors in a differential configuration using commercial GMR elements inserted on a coil in a ferrite pot. We provide an example of a GMR probe and show that the eddy current probe based on giant magnetoresistance (GMR) is more sensitive than the inductive probe. We introduce the notion of the effective area (EA) of the GMR sensor calculated and optimized using the inverse problem (Particle Swarm Optimization method). We validate the operation of the differential GMR sensor using a 3D finite element model based on the formulation (A, V–A) and experimental measurements.

Finally, we test the prototype of the differential GMR sensor. We are developing a measurement bench in the laboratory for prototyping and then validating the data inversion to evaluate the cracks machined on an aluminum standard. Artificial neural networks are used for data inversion.

The work of this thesis is presented in the form of 4 chapters.

In the first chapter, we present a state of the art of eddy currents non-destructive testing (ECNDT) to situate our problem in its NDT context. We present all the different NDT methods, particularly the ones using eddy currents; we show some sensor functions and their description; only the following eddy current probes are detailed: inductive sensors, fluxgates, magneto-impedances, Hall effect sensors, and magneto-resistive sensors.

The second chapter is a presentation of the tools of software and hardware tools for the design of the high-sensitivity magnetic sensors (GMR probe) in eddy current non-destructive testing.

The third chapter is devoted to the numerical modelling of the emerging crack. The laws of electromagnetism govern the interactions in eddy current testing. A synthesis and a comparison of the different magneto dynamic models for calculating eddy currents in cracked conductive materials are presented. This analysis will lead us to the proposed choice. We present the difficulties of crack modelling due to scaling problems.

In this chapter, we propose new design identification of a mono-element giant magnetoresistance (GMR) probe and a new concept of a differential GMR measurement probe. Also, we present the measurement strategy of the realized prototype with their experimental results and the validation of simulation results.

The fourth chapter is devoted the characterizing cracks using the inversion technique. A data inversion carried out by a neural network thus allows us to characterize an emerging defect. It, therefore, constitutes the last link in the overall crack characterization strategy.

Thus, the chapters of this thesis are titled as follows:

Chapter 1: High sensitivity magnetic sensors in Eddy Current non-Destructive testing

Chapter 2: GMR probe design: Simulation in eddy current non-destructive testing (EC-NDT) system

Chapter 3: GMR probe construction: Experimentation and prototyping

Chapter 4: GMR probe application: Data inversion

CHAPTER 1

High sensitivity magnetic sensors in Eddy Current non-Destructive Testing

Contents

1.1. Introduction

This chapter proposes state-of-the-art eddy currents non-destructive testing (ECNDT) to situate our problem in its NDT context. Non-destructive testing is a set of methods that characterize the industrial structures' integrity without degrading them, either during production (the parts that leave the foundries are never free of defects) or during their use.

Firstly, we present all the different NDT methods, particularly the ones using eddy currents. Next, we show the different types of sensors in EC-NDT applications and their excitation modes.

Finally, we show some eddy current probes functions and their description. Its implementation is already the subject of important work in our laboratory. Thus, only the following eddy current probes are detailed: fluxgates, magneto-impedances, Hall effect sensors, and magneto-resistive sensors.

1.2. The different NDT techniques

NDT is a unique technique save money and time in product evaluation, troubleshooting, and research. The six most frequently used NDT methods are [Zerguini 09]:

• Penetrant testing.

• Magnetic particle testing.

• Ultrasonic testing.

• Eddy currents.

• Thermography.

• Radiography.

1.3. Different types of sensors

The excitation provides in practice by a coil, which is generally circular, and supplied with a variable voltage or current. We distinguish several types of sensors:

1.3.1. Double function probe

The dual-function sensor consists of a single coil (transmitting- receiver). The identical windings perform their excitation and reception functions. [Helifa 12, Abdelli 14]. The magnetic field of the reaction varies according to the circulation of EC in the material [Abdelli 14] (Fig.1.1).

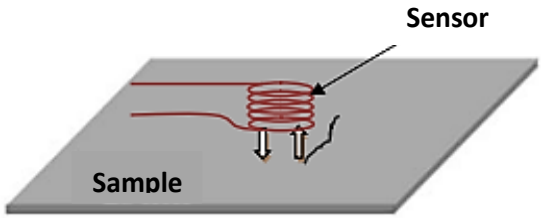

Fig 1.1 double fonction probe.

1.3.2. Separate function probes

In the case of the sensor with a separate function, there are at least two coils. One is reserved for the creation of the magnetic field of excitation. The second coil, small in size, represents the measurement voltage coil. This technology is used when the control requires intense magnetic fields; it is used for low-frequency contr 1kHz) [Helifa 12, Zerguini 09]. The measuring element can be a coil or magneto-resistive Hall effect sensor [Choua 09]. (Fig.1.2).

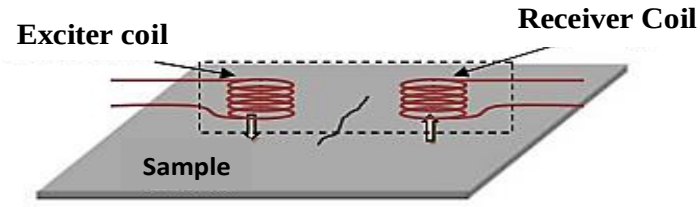

Fig 1.2 Separate function probe

1.3.3. Differential probes

This coil detects discontinuities as it moves along a part while avoiding induced disturbances according to the variations in the coil-sample distance [Zemouri 16] (Fig.1.3). In these devices, the sensor consists of at least two rigidly linked elements [Zemouri 16]. They are intended to access only local variations in the product characteristics examined by the permanent difference of two simultaneous measurements in two neighboring zones [Abdelli 14].

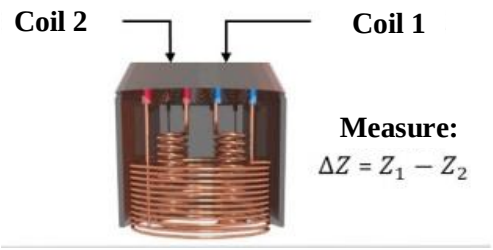

Fig 1.3 Differential probe.

1.4. Different modes of excitation

The extraction of information on the sample to be checked is related to the excitation mode of the sensor [Lakhdar 11]. The sensitivity of the method depends on the frequency of the excitation current. We can distinguish three excitation modes for eddy current sensors: single-frequency excitation, multi-frequency excitation, and pulsed excitation. [Lakhdar 11, Delabre 16].

1.4.1. Single frequency excitation

In single-frequency control, a coil generates the magnetic field or inductor supplied by a sinusoidal current and fixed frequency [Choua 09, Delabre 16]. The conductive characterization sample obtains by measuring the variation in the excitation coil's impedance compared with that measured in a vacuum. The choice of the frequency value depends on the intended application [Zerguini 09].

Low-frequency eddy currents are suitable for testing very thick products and ferromagnetic materials.

1.4.2. Multi-frequency excitation

The multi-frequency method is the most widely used in the field of eddy current NDT. [Zemouri 16]. It is used for inverting the data provided by the probe to determine the parameters of the facing material [Choua 09]. The principle of multi-frequency excitation is to feed successively, or simultaneously, the coil at several different frequencies. This excitation can free single-frequency excitation from disturbing parameters because the information materials (electrical conductivity, magnetic permeability, air gap, or default dimensions) are potentially enriched by the different frequencies used [Delabre 16]. These parameters can be of different types [Choua 09, Helifa 12]:

- Probe / target distance (lift-off).
- Electrical conductivity of the target (σ).

- The magnetic permeability of the target (μ).
- Defects in the material.- thickness of the material to be checked.

1.4.3. Pulse excitation

Pulsed excitation is an alternative to multi-frequency excitation. In this case, the transmitter is excited with a pulse signal, finite duration, and rich spectral content, which can be of different shapes, such as rectangular, triangular, or half-sinusoidal. Pulsed excitation sees utility in the inspection of buried defects, the measurement of thickness, or the measurement of electromagnetic parameters of materials. The implementation of Pulse excitation to evaluate the application of metal coating thickness is applied to detect deep defects [Chou 09, Thollon 95, Bour 96]. [Zemouri 16, Delabre 16].

1.5. Standard impedance plane

An inductive sensor (a winding of N turns traversed by a sinusoidal alternating current I_{exc}) is characterized by two quantities:

- The resistive component R includes eddy current losses due to the penetration of the field into the target. In addition, the internal losses of the excitation winding.
- The inductive term X represents the reactance of the excitation winding. It is linked to the topology of the magnetic field lines emitted by the probe. [Santandréa 10, Helifa 12, Abdelli 14, Choua 09].

$$Z = \frac{V_{exc}}{I_{exc}} = R + jX \tag{1.1}$$

To keep in the expression of the impedance only the variations due to the presence of the target, to eliminate the components of impedance under vacuum X_0 and R_0 ($Z_0 = R_0 + jX_0$), we introduce the concept of normalized impedance defined by:

$$Z_n = \frac{Z - R_0}{X_0} = R_n + jX_n = \frac{R - R_0}{X_0} + j\frac{X_c}{X_0} \tag{1.2}$$

Standardization made the measurement independent of specific characteristics of the coils (number of turns, no-load losses) and the growth of the reactance as a function of the frequency. It depends on the following:

- ✓ The structural parameters: the excitation frequency f and the sensor's geometry.
- ✓ The sensor-sample distance (lift-off).

✓ The geometric parameters of the sample. [Abdelli 14, Helifa 12, Doirat 07]

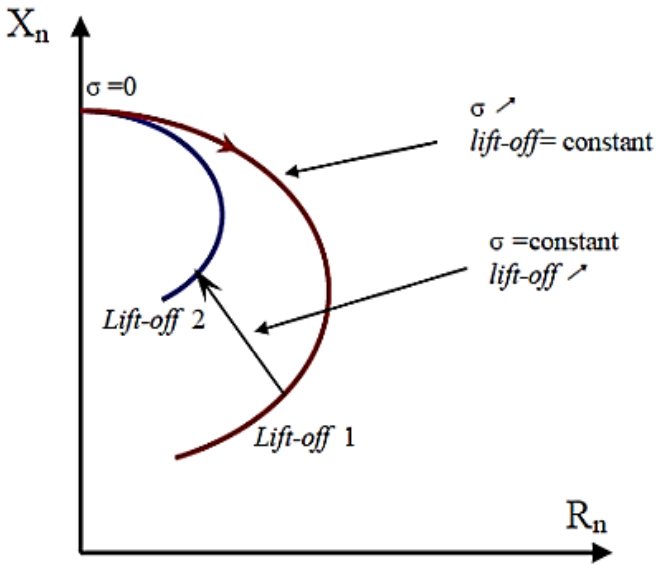

Fig 1.4 Influence of conductivity and lift-off on the normalized impedance diagram.

1.5.1. Skin effect

The intensity of eddy currents in a conductive material characterized by electrical conductivity σ and magnetic permeability μ decreases with depth (Fig.1.5). In EC-NDT, defects are detected up to a few. The conventional depth of penetration δ describes this effect, often referred to as skin thickness. The thickness of the skin is given by:

$$\delta = \sqrt{\frac{1}{f\ \pi\sigma\mu_0\mu_r}} \tag{1.3}$$

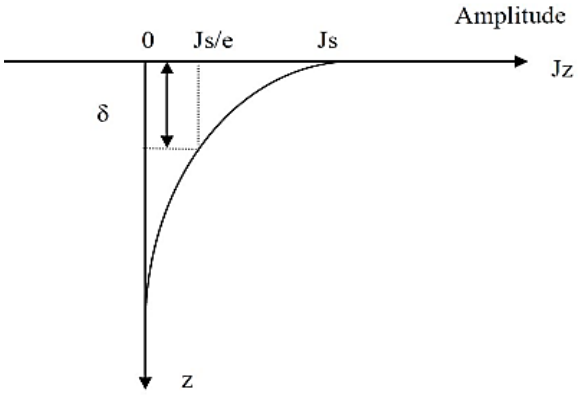

Fig.1.5 Distribution of eddy currents in a part depending on the depth z

We consider a flat piece of infinite thickness excited by an external current of frequency *f* (in Hz). It is shown that 63% of the current flows through the skin thickness. The current density module in the room is [Choua 09]:

$$J(Z) = J_Z e^{-\frac{z}{\delta}} \tag{1.4}$$

Where z is the depth of the sample, J (z) is the current density module at z depth, and J_s is the current density module at the sample's surface (z = 0). We can see that the current density decreases exponentially in the example (Fig.1.4) [Abdelli 14].

1.6. Tension plan

When using a separate function sensor, it is not measured by the impedance but by the complex voltage U [V] across the receiver element. This voltage is referred to as an electromagnetic force or e.m.f. It is first necessary to define a phase reference. For example, the excitation current of the transmitter coil. The expression of this voltage when the receiver is the air is written as:

$$U = U_0 = \mathrm{Re}(U_0) + j\ \mathrm{Im}(U_0) \tag{1.5}$$

Where $\mathrm{Re}(U_0)$ and $\mathrm{Im}(U_0)$ represent the real and imaginary [V] parts of the e.m.f, respectively, across the receiver into the air in the presence of a conductive sample, the e.m.f becomes:

$$U = U_{Sample} = \mathrm{Re}(U_{Sample}) + j\ \mathrm{Im}(U_{Sample}) \tag{1.6}$$

The expression of the normalized voltage at the terminals of the receiver can be defined by:

$$U_{NORM} = \frac{U_{Sample} - \mathrm{Re}U_0}{\mathrm{Im}(U_0)} \tag{1.7}$$

In the case of a sensor with separate functions, and a coiled receiver and the excitation current as a phase reference, $\mathrm{Re}(U_0)$ is zero, and the equation (1.6) becomes:

$$U_{NORM} = \frac{\mathrm{Re}U_{Sample}}{\mathrm{Im}(U_0)} + j\ \frac{\mathrm{Im}U_{Sample}}{\mathrm{Im}(U_0)} \tag{1.8}$$

When the sensor with a combined transmitter and receiver is supplied with current, the definition of U_{NORM} gives a result identical to the standardized Z_{NORM} impedance. The normalized Z and U values are compared in the same complex plane. The points $Z_{(0,1)}$ and $Z_{(0,0)}$ of the impedance plane, after normalization of the measurements, the points are common to the two sensor configurations. Point $Z_{(0,1)}$ represents a measurement of the sensor in air, and point $Z_{(0,0)}$ size in the presence of a material having a conductivity that tends to infinity if the magnetic coupling between the sensor and the material is perfect [Delabre 16].

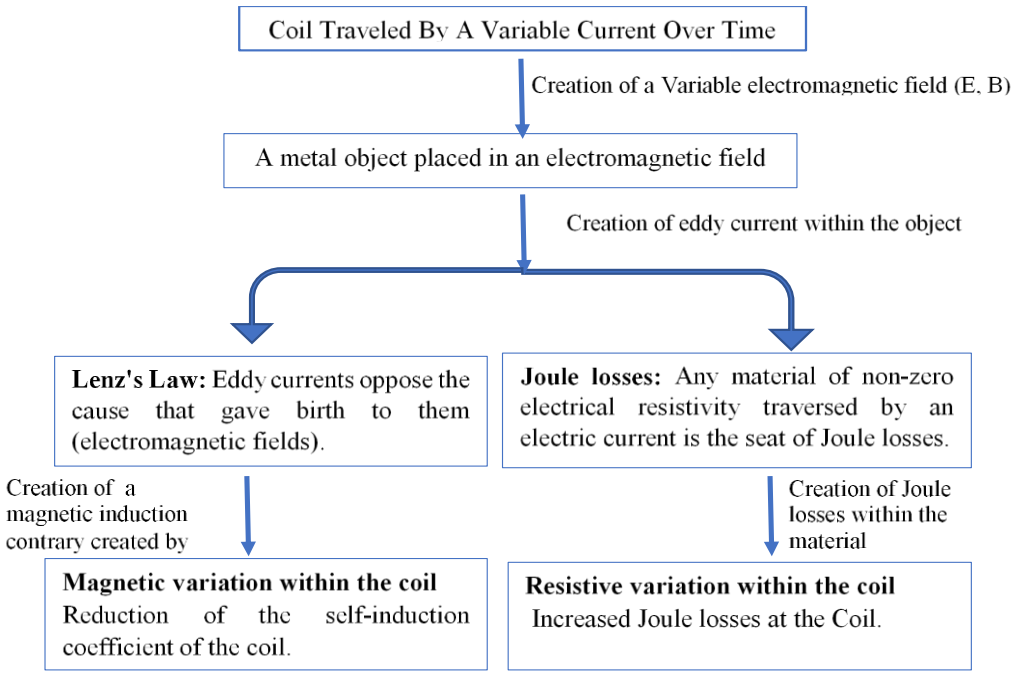

Fig 1.6 Principle of the impedance coil variation following the eddy currents generation.

1.7. Inductive sensors

The operation of these sensors is based on the phenomenon of electromagnetic induction: an electromotive force *e* is induced in a closed circuit subjected to a magnetic flux (resulting from a variable magnetic installation). The Lenz-Faraday law allows calculating this electromotive force *e*:

$$e = -\frac{d\varphi(t)}{dt} \tag{1.9}$$

Where φ is the flux of the magnetic field passing through the closed circuit, the sensors most commonly used in NDT are the coils «wired » [Vacher 07, Moulder 92]. They usually consist of a copper coil wire wrapped around a core made of air or ferrite. Their design is the simplest to achieve and the least expensive; those characteristics are interesting for industrial applications [Zorni 12].

1.8. Eddy current probe

1.8.1. Fluxgates

Fluxgates are developed for the manufacture of compass navigation systems. They consist of a ferromagnetic core and a minimum of two windings. The first coil is the excitation coil, while the second winding is the measuring coil. The principle of operation of these sensors exploits the saturation of a ferromagnetic material. Fluxgates can provide field sensitivities of the order of a few tens of nano Tesla. The excitation field and the response time of the ferromagnetic material limit the sensor response frequency. The upper limit of the frequency is approximately 1 kHz. (Fig 1.7) [Lenz 06].

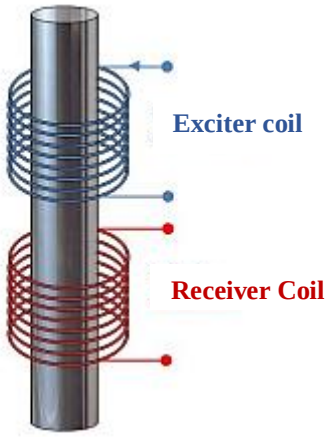

Fig 1.7. Fluxgate sensor consisting of a ferromagnetic core and two coils. In blue is the excitation coil and in red is the measurement coil.

1.8.2. Hall effect sensors

The principle of the Hall effect sensor is described in the case of a conductive material and, more importantly, in semiconductor materials to illustrate the principle. We consider conductive materials for simplicity. When a conductive track (the thickness is generally between 0.4 and 100μm) travers by a direct current I, applied along the y axis and subjected to a magnetic induction B used in this example along the z-axis, there appears a potential difference *VH* in the direction perpendicular to that of the induction and the current. i.e., the y-axis. (figure 1.8) This so-called Hall voltage is due to the Lorentz force and is given by [Zorni 12, Lenz 06]:

$$F = qv \wedge B \tag{1.10}$$

Where *q* is the charge of the electrons and *v* is their speed (Fig 1.8).

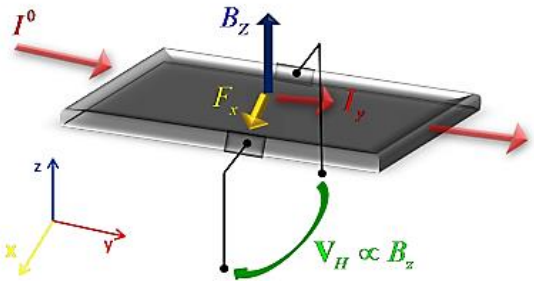

Fig I.8 Principle of Hall effect sensors.

1.8.3. Magnetoresistors

A magneto-resistance is a magnetic sensor; it is transformed by a variation in magnetic field B into a variation in resistance R. All conductors exhibit a magneto-resistive effect. It is typically too weak to be used as a field sensor. Many magnetic materials exhibit a more significant magneto-resistive effect known as anisotropic magneto-resistance (AMR), which is substantial enough to be used in sensors. Thus, recent advances in technologies and materials make it possible to produce devices composed of thin layers with a strong-magneto-resistive effect, such as giant magneto resistors (GMR) and tunnels (TMR). The rate of MR is defined as follows:

$$MR(\%) = \frac{R_{\max} - R_{\min}}{R_{\min}} \tag{1.11}$$

Where R_{max} and R_{min} are the maximum, and minimum resistance reached when the magnetic field varies. In the case of AMRs, this factor is typically 1% - 2% for GMRs 20% - 60% and TMRs 50-60%) [Baibich 88, Smith 99].

1.8.4. Giant magnetoresistors

Two types of giant magneto resistors are distinguished by the number and nature of the metallic layers used. Giant magneto- resistors (GMR) consists of a stack of layers of conductors and ferromagnetic materials [Reig 13]. The first giant magnetoresistance of this type was discovered simultaneously in Orsay by Albert Fert in 1988 [Jander 05, Reig 13] and Germany by Peter Grünberg [Reig 13] and consisted of a stack of layers of iron 3nm thick with layers of Chromium 0.9nm thick.

1.8.4.1. The first type

It consists of an alternating stack of ferromagnetic layers with non-magnetic conductive layers.

- The magnetization axes of the successive ferromagnetic layers are opposite without an external magnetic field. (figure 1.9)
- In the presence of a magnetic field, the magnetization axes of all magnetic layers gradually align with the axis of the applied magnetic field.

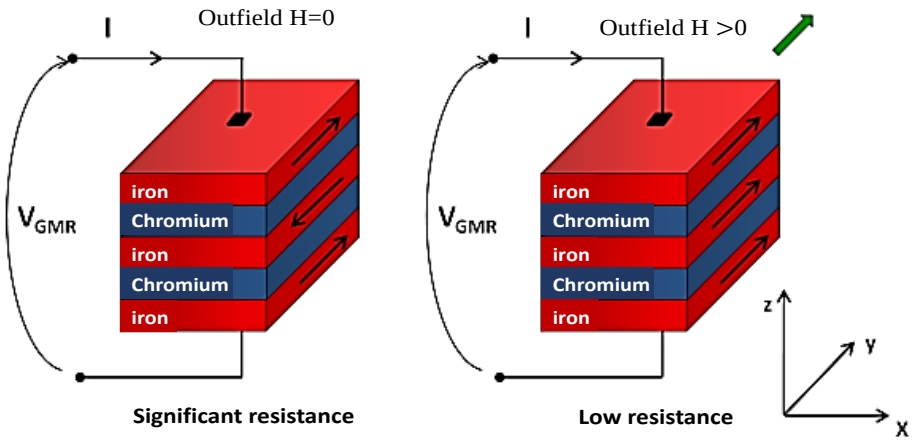

Fig 1.9 Magnetoresistance made up of a stack of Iron / Chromium layers.

NiFe (2.5nm) /Ag(1.1nm) multilayers produce magnetic sensors with weak saturation fields and exhibit variations in resistance of around 15%. The changes in magnetic layers' orientation are accompanied by a decrease in the electrical resistance of the multilayer. Figure 1.10 shows the historical result obtained with such layers at 4K. Unfortunately, this structure's saturation field (~ 1 Tesla) is too large to realize efficient magnetic sensors.

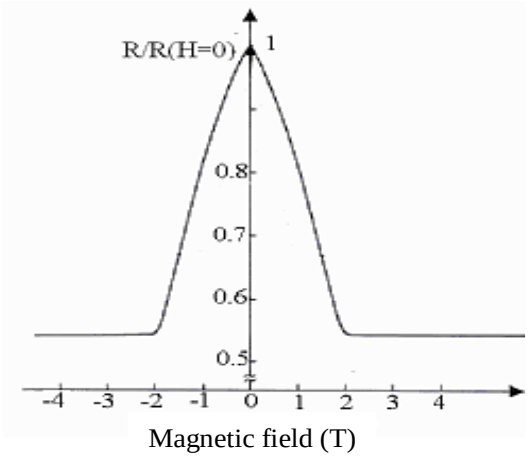

Fig 1.10 Normalized resistance variation R / R (H = 0) as a function of the magnetic field B of the first GMR carried out in 1988 [Baibich 88].

1.8.4.2. The second type

The second type of magneto-resistance is used: spin valves. These are magneto resistors-magneto resistors using only two ferromagnetic layers. (Fig.1.11)

- We trap one of the ferromagnetic layers' orientation and keep a fixed direction; this "hard" layer of magneto-resistance.
- Another ferromagnetic layer retains its ability to change orientation depending on the direction of the magnetic field applied to the magneto-resistance: This is the "soft" layer.

When the magnetization of the soft layer changes orientation, the resistance of magneto-resistance changes; resistance variations up to 25% have been measured in spin-valve compounds, while these variations do not exceed 15% in multilayer GMR. [Smith 99].

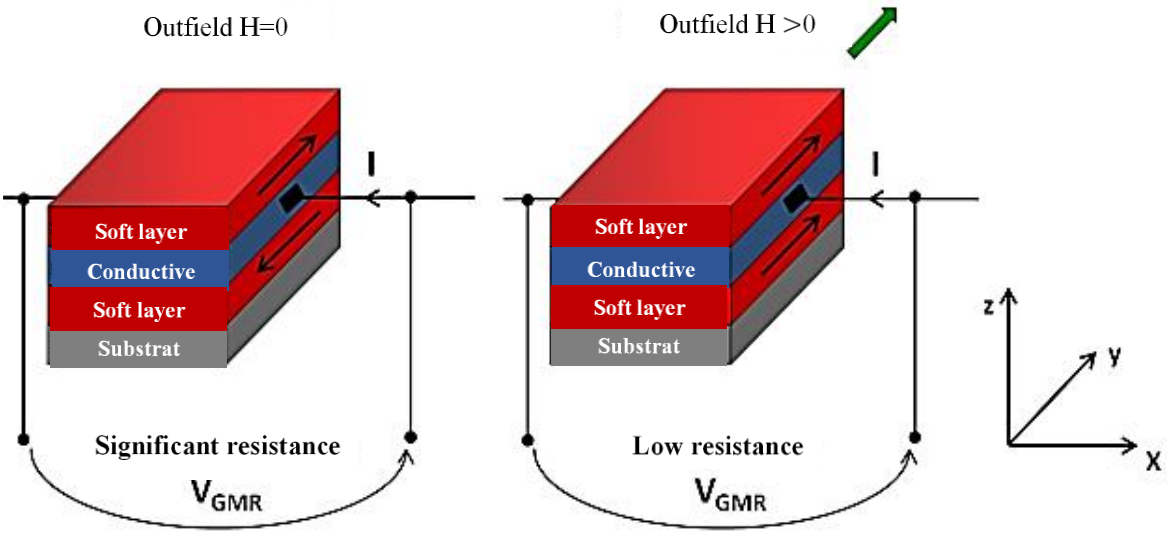

Fig 1.11 Magnetoresistance with spin valves, consisting of a "soft" layer and a "Hard" separated by a conductive film. The substrate is used to fix the orientation of the "hard" layer magnetization.

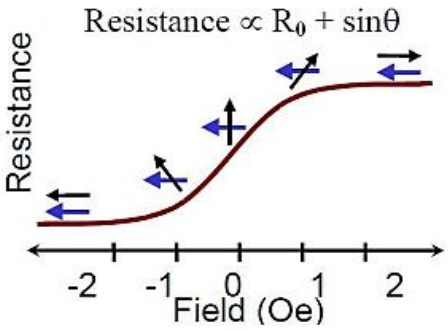

Fig 1.12 Variation of the resistance of a spin valve GMR as a function of the applied magnetic field. The blue and black arrows represent the orientation of the spins of two layers «hard and soft» respectively. The resistance is proportional to the angle θ between the magnetizations of the two layers [Jander 05]

1.8.4.3. The physical origin of the giant magnetoresistance phenomenon

The magnetic properties of a material are of microscopic origin at the atomic level. An atomic moment *mi* is made up of an orbital moment for each atom (the rotation of electrons on an orbit around the nucleus) and a spin moment (the process of electrons around the proper axes); figure 1.13 schematizes the atomic moment. Spin is a quantum property intrinsic to any particle. It is used as a discriminating factor for electric carriers and quantified according to two opposite values, +1/2 (ou *up*) and -1/2 (ou *down*). Subject to an external magnetic field, the atomic moments align with it under the action of the couple:

$$\Gamma = \mu_0 m \times H \tag{1.12}$$

The magnetic moment M of the material (in Am^2) is given by the sum of all the atomic moments $M = \sum_{i=1}^{n} m_i$. If the moments are randomly oriented (M), the material is in a demagnetized state. The material is magnetized if they are collectively introduced (M ≠ 0). The magnetization M of material of volume V is given by:

$$m_i = \frac{M}{V} \tag{1.13}$$

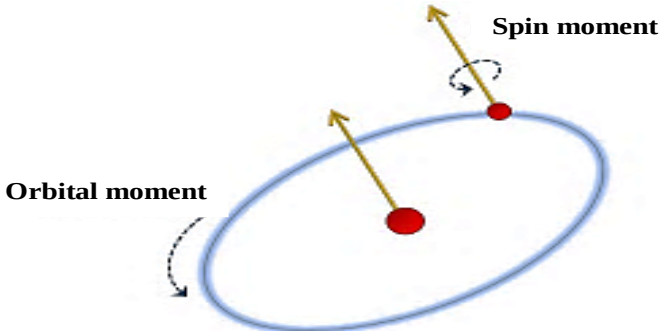

Fig 1.13 Illustration of the atomic moment.

1.8.4.4. Magnetic Domains of nanolayer magnetic

To illustrate the principle of GMR sensors, we consider two configurations characterized by a stack of ferromagnetic layers with parallel magnetization. see figure 1.14a and antiparallel, see figure 1.14b [Iorio 07].

In both cases, a non-magnetic conductive layer is inserted between the two ferromagnetic layers. The electrons that take part in electrical conduction spin up or down compared to the layers. The electron's trajectories are determined by their spin; the diffusion phenomena are vital in the case of a spin parallel to the magnetization and weaker in the opposite case.In the configuration with parallel magnetizing layers, the spin-up electrons pass through the structure almost without diffusion (green arrow). In contrast, the spin-*down* electrons are more strongly diffused (red arrow). We can write the equivalent resistance of the structure by calling r the resistance encountered by the electron in the magnetizing layer parallel to its spin and R the resistance encountered when passing through an antiparallel layer. We can schematize the trajectories of two electrons of opposite spin with four resistances. The equivalent resistance R‖ is worth in this configuration:

$$R_{\parallel} = 2\frac{rR}{r+R} \tag{1.14}$$

$$\cong 2r, \quad if \quad R \gg r \tag{1.15}$$

In the antiparallel configuration, the electrons are all scattered. Therefore, the resistivity of the structure is higher.

$$R_{\neq} = \frac{R+r}{2} \tag{1.16}$$

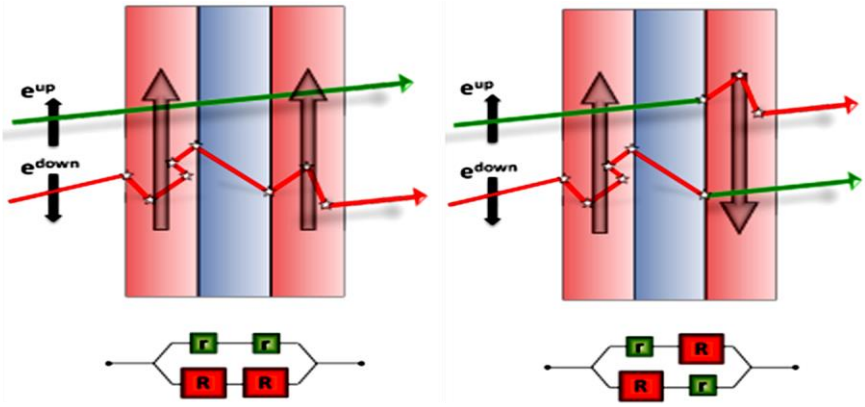

(a) Parallel multi-layer configuration (b) Antiparallel multi-layer configuration

Fig 1.14 Operating principle of the giant magnetoresistance [Reig 13]

1.8.4.5. The performances of giant magnetoresistors

GMR technology is preferred for producing phased array sensors with a spatial resolution of less than 100µm. A strong point of this technology is the ease of manufacturing phased array sensors. These sensors are interesting for producing NDT probes.

The company NVE Corporation (NVE) also markets GMRs encapsulated in boxes whose dimensions vary according to the model. For example, a GMR NVE of the AAH series using a SOIC8 box occupies a volume of (4 × 5 × 1.5) mm^3, as shown in figure 1.16. Inside the case, four GMR, two active and two inactive, are mounted as a Wheatstone bridge to eliminate temperature drifts. Ferrite flux concentrators are integrated within the chips to amplify the measured magnetic field (figure1.15).

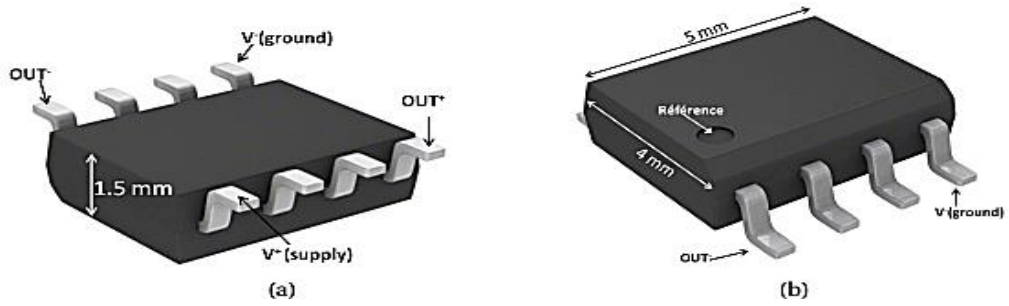

Fig 1.15 Characteristic dimensions of an NVE AAH series commercial GMR [catalog 21]

1.9. Advantages of Eddy current NDT

The NDT by EC:

- It does not require coupling products; it makes it easier to use. Similarly, no pollution or nuisance is generated for the user or the environment, unlike, for example, penetrant testing, which is widely used and requires the application of harmful chemicals.
- Transportability: NDT-EC does not require bulky equipment and can be performed in hard-to-reach places with portable equipment. In addition, testing at high temperatures is possible [Choua 09].

1.10. Limitations of Eddy Current NDT

- The interpretation of signals is often complex.
- It is only applicable to electrically conductive materials.
- It is not adapted to detect defects at great depth.

1.11. Conclusion

This chapter present a general overview of nondestructive testing techniques in which eddy-current sensors occupy an increasingly important place. Magnetic sensors coiled on wires are used in conventional NDT probes. Indeed, they are robust, easy to use, and allow contactless measurements; from the impedance measurement of this type of sensor.

This section is explored various eddy currents probes technologies for use in nondestructive testing. It is examined to employ fluxgates, magneto-impedances, Hall effect sensors, or even Giant Magneto Resistance in NDT to enhance the performance of traditional NDT probes.

CHAPTER 2
GMR probe design: Simulation in eddy current non-destructive testing (EC-NDT) system

Contents

2.1. Introduction

Non Destructive Testing (NDT) is to detect and evaluate the size of cracks in critical parts of industrial devices [Helifa 16a]. The current challenge lies in detecting smaller and smaller defects while reducing the inspection time. Inductive sensors are the most commonly used in eddy currents non-destructive testing (EC-NDT). Their high sensitivity in EC-NDT systems allows for improved performance in detecting deep cracks [Hamia 13]. Nevertheless, low-frequency eddy current (ECT) controls require sensors with high field sensitivity and spatial resolution [Hamia 10].

To exceed the performance of wire wound sensors in sensitivity and resolution. We use giant magneto-resistance (GMR) [Rifai 16, Bernieri 19], characterized by high sensitivity. Low frequency, making them suitable for many practical applications, including crack assessment [Rifai 16, Smith 04], wide dynamic range, and are relatively easy to realize and cheap [Zorni 12, Dogaru 01], which is suitable for many practical applications, including crack assessment [Rifai 16, Smith 04].

GMR sensors in the field of NDT have triggered the development of very sensitive probes [Dogaru 01, Gao 18]. For example, authors such as E. Ramírez-Pacheco [Ramirez 10] developed an experimental eddy current (EC) system to characterize near-side cracks in Aluminum by slightly moving the GMR sensor concerning the center of the excitation coil. In [Romero 20], Romero-Arismendi analyzed the influence of design parameters on the sensitivity of the GMR-based sensor. Nevertheless, GMR sensors for NDT applications are still under development; in the pre-mentioned work, the probe's sensitivity regarding its design parameters is not fully characterized to address these constraints and investigate a new sensor design.

We describe the problem and Maxwell's equations. After that, the associated boundary conditions. Then, we present the different magnetic formulations for such a problem, also the formulation used for our 3D model. We focus on the finite elements method (FEM) in our work. This method is based on transforming partial differential equations (PDE) into a system of algebraic equations. Generally, solving a magnetic problem given by FEM involves several steps. The whole summarizes in figure 2.1.

This work approach uses two symmetric giant magneto-resistance sensors in a differential configuration using commercial GMR elements inserted on a ferrite pot coil. First, the area of action of the commercial GMR sensor is evaluated using the inverse problem method that minimizes the difference between the calculated and measured magnetic field strength using the particle swarm optimization (PSO) algorithm. The operation of the differential GMR sensor is

validated through a 3D Finite Element Model (FEM) based on (A, V-A) formulation and experimental measurements.

Finally, the model is created with the same experimental characteristics in the same conditions as the experimental case studies. All the simulations are performed using a Finite Element method FEM software, ANSYS Electronics, Z9PE-D8 WS solver on a 12-core Processor Intel® Xeon ® CPU E5-2620 at 2.00 GHz. with 128 GB RAM.

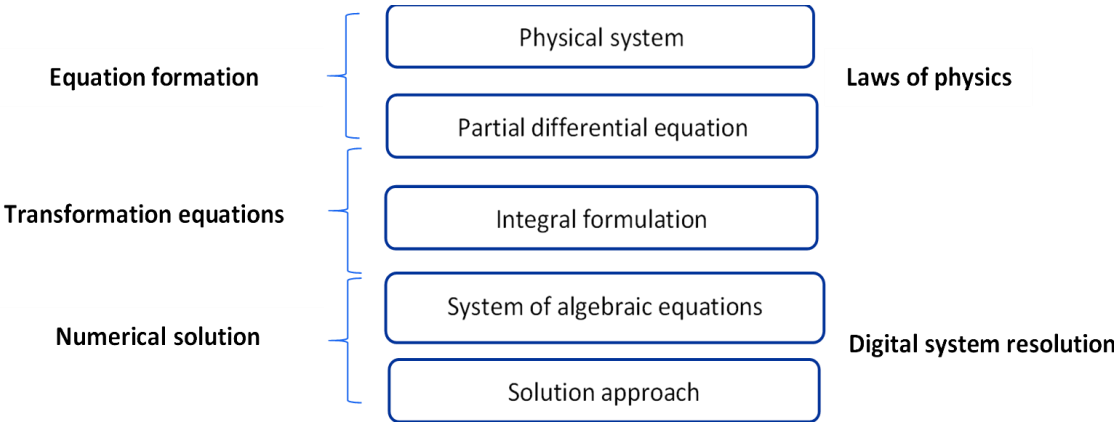

Fig 2.1 Presentation of the different stages of numerical resolution of a problem by the EFM.

2.2. Typical problem in EC-NDT

The electromagnetic problem is treated and put in the form of the principle diagram; It's to solve Maxwell's equations in a linear harmonic regime. The geometries are generally composed of the following parts. Figure 2.2 represents a typical eddy current problem. Indeed, the EC-NDT implement involves an inductor coil (coil, wire, etc.) in a non-magnetic electrically conductive sample (conductors where induced currents can flow). In addition, the global domain represents the resolution domain of the electromagnetic problem, where boundary conditions impose on its border Γ [Bensetti 08, Doirat 07, Choua 09]. An air box encompasses an inductor in which a source current density Js circulates and a permeability conductor μ and conductivity σ.

The objective is to evaluate the spatial distribution of the electric field and magnetic induction in the global domain.

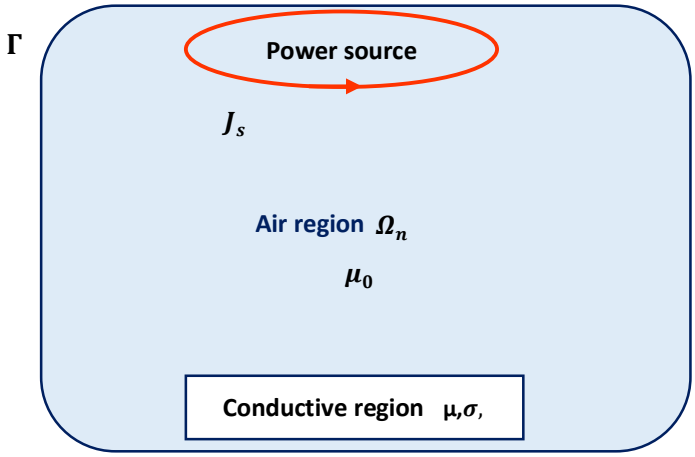

Fig 2.2 Typical magnetodynamic problem

2.3. Maxwell's equations

Maxwell's equations are the general model that describes the performance and interactions of electric and magnetic fields and their respective sources' loads and current densities. They reflect the interdependence of these four quantities' constitutive relations. The differential equations form as follows [Gardiol 02]:

$$div\,\vec{D} = \rho \qquad \text{Gauss' theorem} \qquad (2.1)$$

$$div\vec{B} = 0 \qquad \text{Conservation law of magnetic flux} \qquad (2.2)$$

$$\overrightarrow{rot}\vec{E} = -\frac{\partial \vec{B}}{\partial t} \qquad \text{Faraday law} \qquad (2.3)$$

$$\overrightarrow{rot}\vec{H} = \vec{J} + \frac{\partial \vec{D}}{\partial t} \qquad \text{Ampere-Maxwell theorem} \qquad (2.4)$$

$\vec{E}$[V/m], $\vec{B}$[T],J[A/m2], and ρ[C/m3] are, respectively, the electric field, the magnetic induction, current density, volume density of electric charges [Kuczmann 09] . To these equations must be associated the behavior laws:

$$\vec{J} = \sigma\vec{E} \qquad (2.5)$$

$$\vec{B} = \mu\vec{H} \qquad (2.6)$$

$$\vec{D} = \varepsilon\vec{E} \qquad (2.7)$$

$\vec{H}$ [A/m] $\vec{D}$ [C/m^2], σ [S/m], μ [H/m], and ε [F/m] are, respectively, the magnetic field, the electrical induction, the conductivity of the inspected material, the magnetic permeability, the permittivity or the electric permeability. These equations globally describe all electromagnetic phenomena. However, it isn't easy to consider all these equations for a complete resolution. Moreover, certain phenomena become negligible depending on the devices studied, and the equations are decoupled. The diagram of figure 2.3 illustrates the coupling between the electric and magnetic phenomena [Bouchala 08] that Maxwell was able to join under the same theory known as "Electromagnetism."

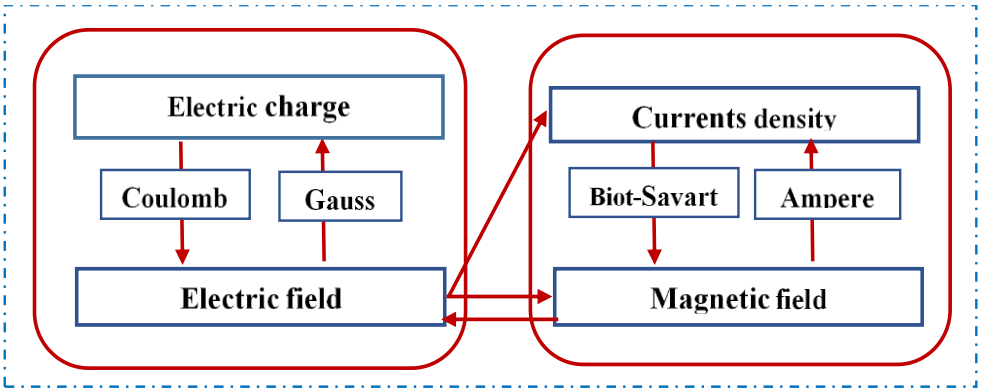

Fig.2.3 coupling between electrical and magnetic phenomena

In this thesis, we are only interested in the formulation of potential magnetic vector and scalar electrics (A, V) types. To simplify EC-NDT problems related to the low-frequency magnetic dynamic model in a quasi-static system, thus displacement current is negligible compared to the conduction current [Abdelli 14, Bouchala 08]:

$$\frac{\partial \vec{D}}{\partial t} \ll \vec{J} \tag{2.8}$$

2.4. Magneto-dynamic formulation

Since Maxwell's equations are a system of vectorial differential equations, they are challenging to solve. The physical quantities discontinuity at the interface of regions of different natures and the large numbers of unknowns to be solved. It is necessary to reduce the unknown number and the number of the equations. The resolution involves intermediate vector or scalar amounts, reducing this complexity. It reduces the memory required at the computer level and computing time [Kuczmann 09, Zaoui 08]. There is no real consesnsus on the best formulation. Many methods are proposed using potential or field type variables for 3-D modeling EC-NDT [Rubinacci 08, Bíró 99, Biro 89].

2.5. Principles electromagnetism formulations

There are two categories of formulations based on either the electric field E or the magnetic field H. The first category mainly includes the formulation in magnetic vector potential A. The second category formulations in H or the formulation in ϕ.

2.5.1. The formulation of magnetic scalar and electric vector potentials *AV-A*

Consider Maxwell's equations, which do not contain material source terms (2.2) and (2.3), we can write [Gardiol 02]:

$$\nabla.\vec{B} = 0 \tag{2. 9}$$

So:

$$\vec{B} = \nabla \times \vec{A} \tag{2.10}$$

According to the previous hypotheses, the equations to be solved are:

$$\vec{E} = -\overrightarrow{gradV} - \frac{\partial \vec{A}}{\partial t} \tag{2.11}$$

$$\overrightarrow{rot}\vec{E} + \frac{\partial \vec{B}}{\partial t} = 0 \tag{2.12}$$

$$\frac{1}{\mu}\overrightarrow{rot}\,\vec{B} = J_s + \sigma\vec{E} - \frac{\partial \vec{D}}{\partial t} \tag{2.13}$$

By combining equations (2.8) (2.9) (2.10), the magneto dynamic equation in magnetic vector potential and electric scalar potential is written by [Helifa 12, Biro 89]:

$$\overrightarrow{rot}\frac{1}{\mu}\overrightarrow{rot}\vec{A} + \sigma(-\overrightarrow{gradV} - \frac{\partial \vec{A}}{\partial t}) = J_S \tag{2.14}$$

To this equation is added the conservation of the current density:

$$div\vec{J} = div(-\sigma(\overrightarrow{gradV} + \frac{\partial \vec{A}}{\partial t})) = 0 \tag{2.15}$$

The use of a gauge must ensure the uniqueness of the potential. In A -V, the Coulomb gauge seems to be the most effective [Abdelli 14, Thollon 95]:

$$div\vec{A} = 0 \tag{2.16}$$

A penalty generally introduces this gauge by adding the term.: $-\overrightarrow{grad}(\frac{1}{\mu} div\vec{A})$

We obtain the symmetrical system of electromagnetic equations to be solved, called the *A*-V formulation [Helifa 12]:

$$\overrightarrow{rot}(\frac{1}{\mu}\overrightarrow{rot}\vec{A}) - \overrightarrow{grad}(\frac{1}{\mu} div\vec{A}) + \sigma\frac{\partial}{\partial t}(-\overrightarrow{grad}V - \vec{A}) = \boldsymbol{J}_S \qquad (2.17)$$

$$div(-\sigma(\overrightarrow{grad}V + \frac{\partial\vec{A}}{\partial t})) = 0 \qquad (2.18)$$

Knowing the potentials (*V*, *A*) makes it possible to determine and use the field-potential relations (2.9) and (2.10). To ensure the uniqueness of a system solution (2.1 to 2.7) is necessary to add three types of conditions: continuity conditions, boundary conditions, and gauges.

2.6. Boundary and continuity conditions

The system is composed of Maxwell's equations and constitutive laws admits an infinity of solutions, the boundary conditions given on the domain boundary to ensure the uniqueness of the solution.

The frontier Γ of the study domain Ω is broken down into two complementary regions Γ_E and Γ_H and such that $\Gamma = \Gamma_e \cap \Gamma_h$ and $\Gamma = \Gamma_e \cup \Gamma_h = \varnothing$ (Fig 2.4). The conditions $\vec{n} \times \overrightarrow{E} = \vec{0}$, and $\vec{n} \times \overrightarrow{H} = \vec{0}$, respectively imposed on Γ_E , and Γ_H .

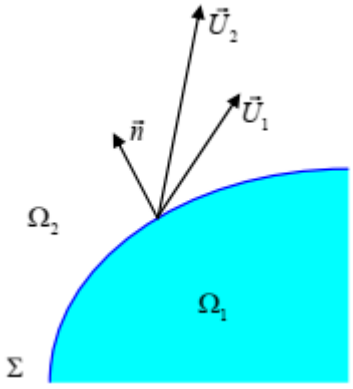

Fig 2.4 Borders Γ_E and Γ_H.

Electromagnetic fields undergo discontinuities when passing between two media with different physical properties. There occur sharp changes in parameters. Let us imagine that it is a surface bounding one medium with material parameters Ω_1 from Ω_2 (Fig 2.5).

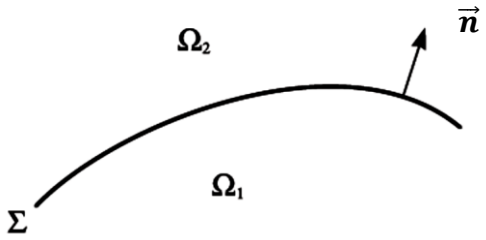

Fig. 2.5 Interface between two media.

For this reason, the transmission conditions between two different media; firstly discontinue the tangential magnetic field component in the presence of surface currents (2.19). Secondly, the standard magnetic induction component is continued at the interface (2.20). Continuity of the tangential electric field component (2.21); finally, electrical induction is discontinued in the presence of surface charges (2.22).

$$\left(H_2 - H_1\right) \times \vec{n} = J_{sur} \tag{2.19}$$

$$\left(B_2 - B_1\right) \cdot \vec{n} = 0 \tag{2.20}$$

$$\left(E_2 - E_1\right) \times \vec{n} = 0 \tag{2.21}$$

$$(D_2 - D_1).\vec{n} = \rho_{sur} \tag{2.22}$$

ρ_{sur}, J_{sur}, $\vec{n}$ are respectively the surface charge density, the current surface density, the vector normal to the surface of separation of the two media Ω_1 and Ω_2, and are directed towards the outside of medium 1. Limiting the domain to study the system for a finite geometry is necessary. Additional conditions on the boundaries of the study field are then required.

2.7. Gauge Transformation

In Maxwell's differential expression, the fields are expressed either up to a gradient (rotational field) or up to the rotational (divergence field), which justifies the use of gauges in some formulations to ensure the uniqueness of the solution. $\vec{U}$ and $\vec{V}$ two vector fields gauge conditions are generally written by:

$$div\vec{U} = 0 \qquad \text{(Coulomb gauge)} \tag{2.23}$$

$$div\vec{U} + K\frac{\partial u}{\partial t} = 0 \qquad \text{(Lorentz gauge)} \tag{2.24}$$

$$\vec{U}.\vec{V} = 0 \qquad \text{(Gauge suitable for edge elements)} \quad (2.25)$$

For example, when a formulation in the vectorial potential uses, the solution is obtained up to a gradient. Therefore, The Coulomb gauge is written by:

$$div\vec{A} = 0 \qquad (2.26)$$

2.8. Numerical resolution based on finite elements

Numerical methods aim to replace a defined problem with a differential mathematical model discrete problem in an algebraic form. In the formulations resulting from electromagnetism physics; we can cite the methods that are more used: finite differences (FDM), finite elements (FEM), Finite volumes (FVM), and boundary integrals (FIM) [Belkhiri 03]. The modeling with finite elements constitutes an exciting approach to optimizing the sensor's structure.

Finite elements adapt well to complex geometries; they make it possible to considerably improve the precision of calculation by considering different types of interpolation functions of the variables. The diversity in the choice of the mesh element gives significant flexibility to the method [Abdelli 14].

2.8.1. Approximation by FEM

The boundary conditions obtain an algebraic system where the vector solution contains the approximate field values on the mesh points. A field discretization consists of the differential equations discretization. The FEM consists of a double discretization. This spatial discretization makes it possible to define essential functions (scalars or vectors) that gave rise to the approximation subspaces of the continuous spaces. [Helifa 12].

To calculate a quantity in a discretized field, several methods of approximation. We can discretize this value:

- With the mesh nodes (nodal approximation).
- By its circulation along the edges of the elements (approximation by elements edges).
- By its flow through the facets of the component.
- By its value at the element volume.

In the electromagnetism field, the nodal element is the most suitable because of the scalar and vector variables, such as magnetic vector potential *A* and the electric scalar potential *V* (continuous through two neighboring elements). For an element e having m nodes, the three components: A_x ,

A_y and A_z of the vector potential magnetic as well as the electric scalar potential V is approximated by:

$$A_s^e = \sum_{j=1}^{m} N_j^e A_{Sj}^e \qquad \text{s = x, y, z} \qquad (2.27)$$

$$V^e = \sum_{j=1}^{m} \alpha_j V_j \qquad (2.28)$$

α_j , N_j^e are interpolation functions

This method is implemented in ANSYS Electronics software and leads to solving algebraic system equations of a matrix form; preconditioning algorithms and iterative processes are necessary to resolve the plan obtained. Thus, we get the approximate values of the magnetic vector potential and the electric scalar potential at each mesh point.

Finally, the classic diagram of the different modeling stages by the finite element method is presented in figure 2.6.

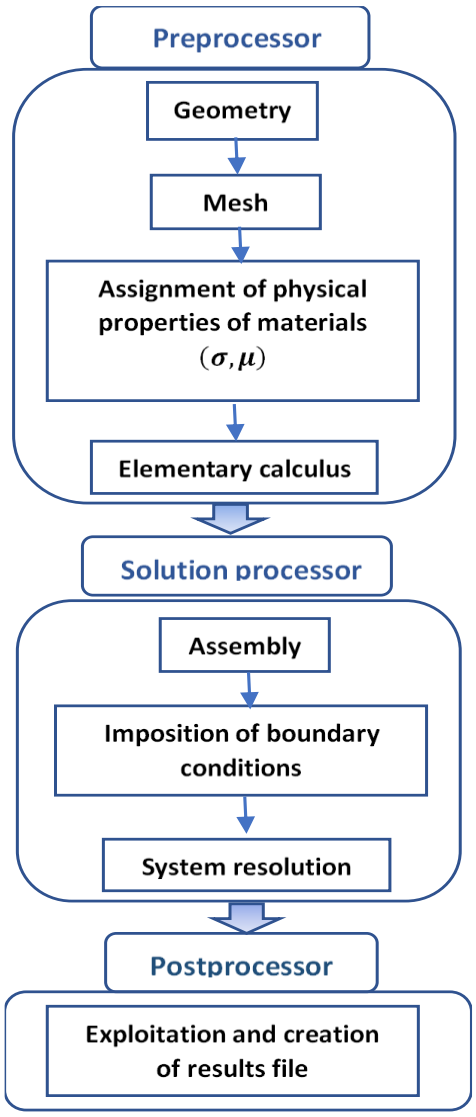

Fig 2.6 Implementation of finite element simulation

2.9. ANSYS Maxwell

ANSYS Maxwell is the first low-frequency electromagnetic field simulation software for engineers responsible for designing and analyzing devices in three electromagnetic and electromechanical 2-D and 3-D, including motors, actuators, transformers, sensors, and coils. ANSYS Maxwell software uses the precise finite element method to solve partial derivative equations to calculate the electromagnetic field and static electric field in frequency and time regime (Fig 2.7).

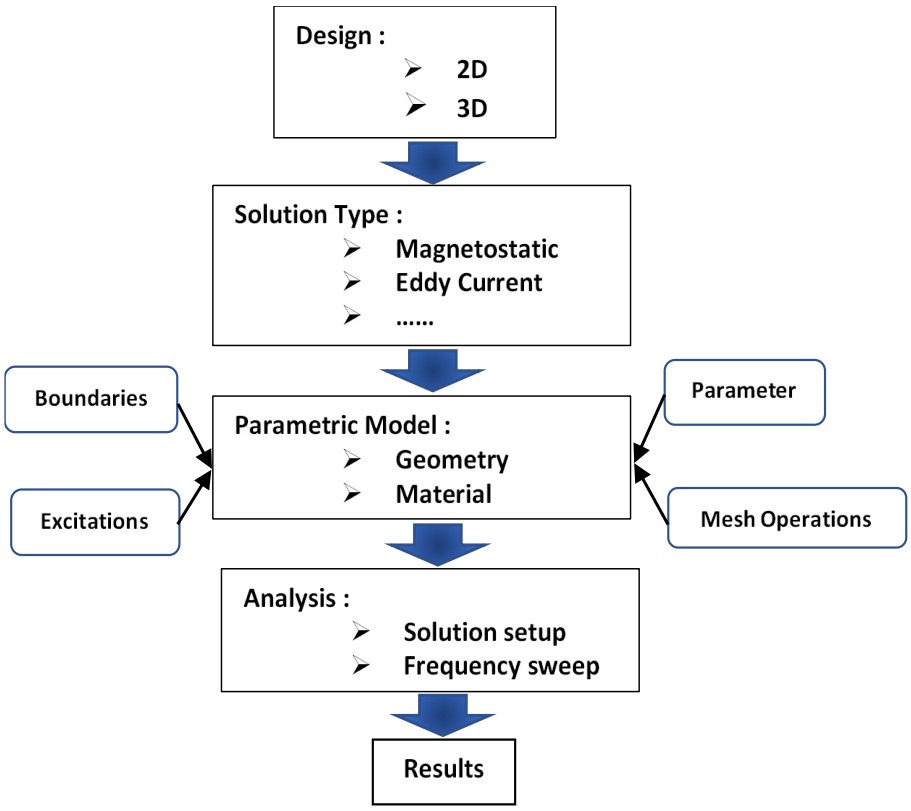

Fig 2.7 Resolution diagram

2.10. Probe Design

The GMR-based eddy current probe's proposed concept is depicted in Figure.2.8 (a). This probe is composed of the previous ferrite coil and two GMR sensors placed beneath it at a distance of 0.1 mm (lift-off) to operate in a differential configuration, i.e., the output of one sensor is subtracted from the other to obtain the probe output. The coil is excited by a sinusoidal current source whose frequency can adjust amplitude. GMR sensors are excited by a constant current source. We focus carefully on choosing the characteristics of the excitation coil according to our knowledge of AAH002-02 GMR sensor proprieties.

The generated magnetic field is sinusoidal in time, as are the eddy currents induced in the Aluminium sample, including the crack shown in Figure.2.8 (b). Therefore, the output voltage is zero for a crack-free Sample. If there is a crack in the sample, the flaw disturbs the eddy current distribution. Since the background voltage is zero, the crack signal is abrupt to the output of the

design probe.

Fig 2.8 Dimensions of the test sample and probe geometry.

2.11. Identification of detectable area by applying Inverse problem to the

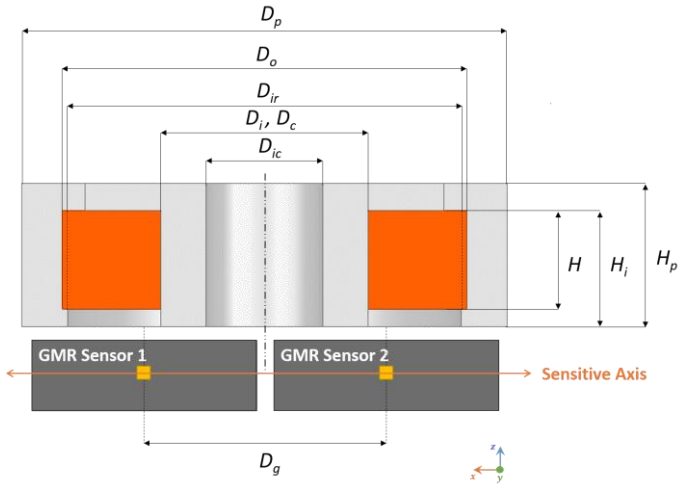

a)

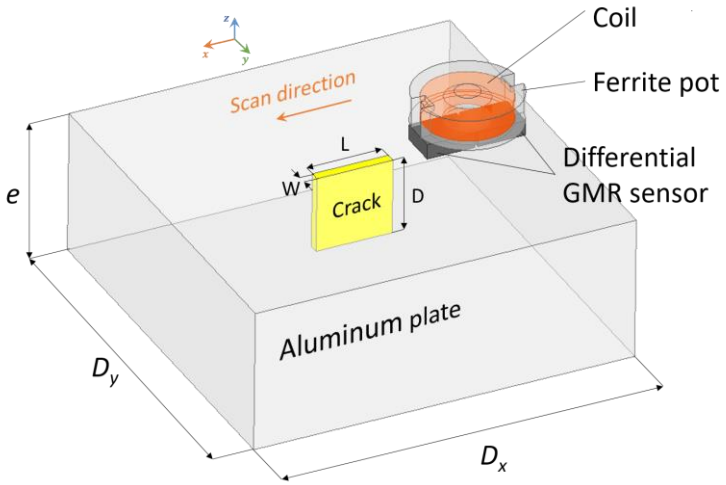

b)

GMR sensor

This section proposes a simple approach to evaluate the detectable area dimensions of the GMR sensor using the inverse problem method. The proposed magnetic field measurement method is direct (the GMR sensor acts as a magnetometer by measuring the magnetic field generated by the permanent magnet). Thus, the magnetic field changes the output voltage on the GMR sensor. Figure 2.9 illustrates the geometric and characteristic dimensions of the numerical model implemented for magnetic field strength calculations of the permanent magnet as a distance function (Axial Magnet). There are two principal parameters of GMR sensor detectable area. The width and the height of the section. The inverse problem goal function is minimized using the

particle swarm optimization (PSO) algorithm to evaluate the detectable area dimensions according to the measurement of the magnetic field strength at the GMR sensor's location.

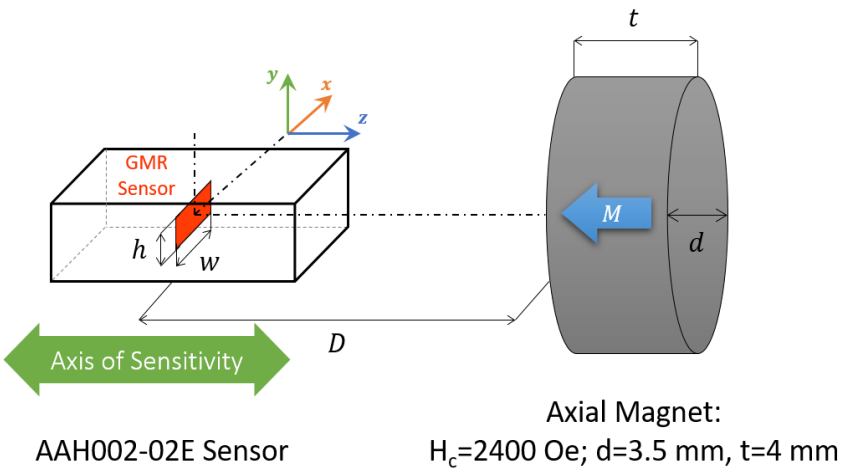

Fig 2.9 Geometric model representing the parameters of the numerical model implemented for magnetic field strength calculations of permanent magnet as a function of distance (Axial Magnet).

A three-dimensional finite element model is used to understand the physical principle and study the performance of the GMR sensor. The model is based on magnetic vector potential $\vec{A}$ formulation, such as: $\vec{B} = curl(\vec{A})$ The equation solved by the finite element method in a Magneto Static application is written:

$$curl\,(V_0\,[V_r\,]curl\,(\vec{A}) - \vec{H}_c) = \vec{0} \tag{2.29}$$

Where$[\upsilon_r]$ is the tensor of the medium's relative reluctivity, υ_0 is the magnetic reluctivity of the vacuum, $\vec{A}$ is the magnetic vector potential, and $\vec{H}_c$ is the coercive magnetic field (permanent magnets). Once the magnetic vector potential $\vec{A}$ is determined, the ''amount'' of magnetic field ''flowing'' through the surface of the GMR sensor is expressed as given by the equation (2.30)

$$B = \frac{\Phi_B}{S} = \frac{1}{S}\iint_s \nabla \times (\vec{A}) \circ \hat{n} da \tag{2.30}$$

Where $\vec{A}$ is the magnetic vector potential, S is the area of the surface, $\hat{n}$ is the unit vector normal to the surface, and da is a tiny area element. In the linear region of the sensor's response, we can express the output voltage as:

$$\Delta U = S_{eff} \cdot B \tag{2.31}$$

S_{eff} is the adequate sensitivity that depends on the sensor type and supply voltage.

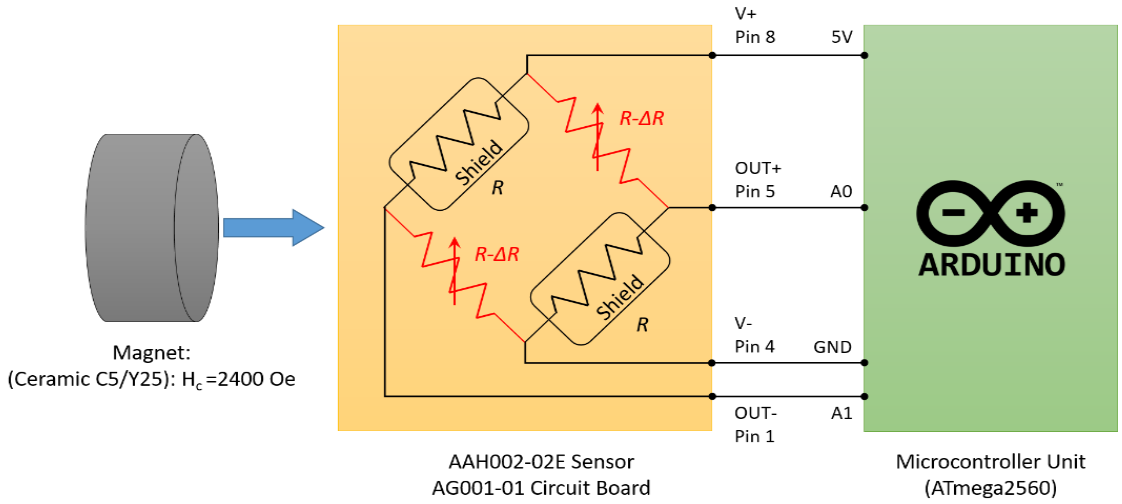

Fig.2.10 Schematic diagram of the experimental setup for magnetic field measurement using GMR sensor.

The magnetic field strength of the permanent magnet is measured using an experimental setup (Fig.2.10) based on a direct microcontroller interface. The magnetic field strength of the permanent magnet is calculated using a 3-D FEM model and then compared with that measured until the convergence criterion of the cost function is satisfied, as represented in (2.32). The detectable area dimensions of the GMR sensor are then identified. The inverse problem algorithm (Fig.2.11) describes these steps.

A particle swarm optimization algorithm is applied to minimize the inverse problem goal function to identify the detectable area dimensions of the GMR sensor. This algorithm is a heuristic search technique that optimizes a problem by iteratively trying to improve candidate solutions concerning a given objective measure of fitness. The inverse problem goal function is written as:

$$\cos t = \frac{1}{2}\left(\frac{B_{mes} - B_{cal}}{B_{mes}}\right) \tag{2.32}$$

Where B_{mes} and B_{cal}, respectively, are the permanent magnet's measured, computed magnetic field strength. The optimal detectable area dimensions of the GMR sensor, using the inverse problem method at a distance value of 18mm from the face of the magnet to the center of the AAH002-02E sensor package, are w = 0.45mm and h = 0.1mm. These values of detectable area dimensions of the GMR sensor are introduced in the 3-D model to compute the magnetic field strength of the permanent magnet as a distance function.

For an AAH002-02E GMR-based sensor S_m*=145(mV/V/mT)*. At a supply voltage V_s=5 (V), one obtains S_{eff} *=725(mV/mT)* and an estimated output voltage ΔU_α=210.25(mV) if D=18 mm.

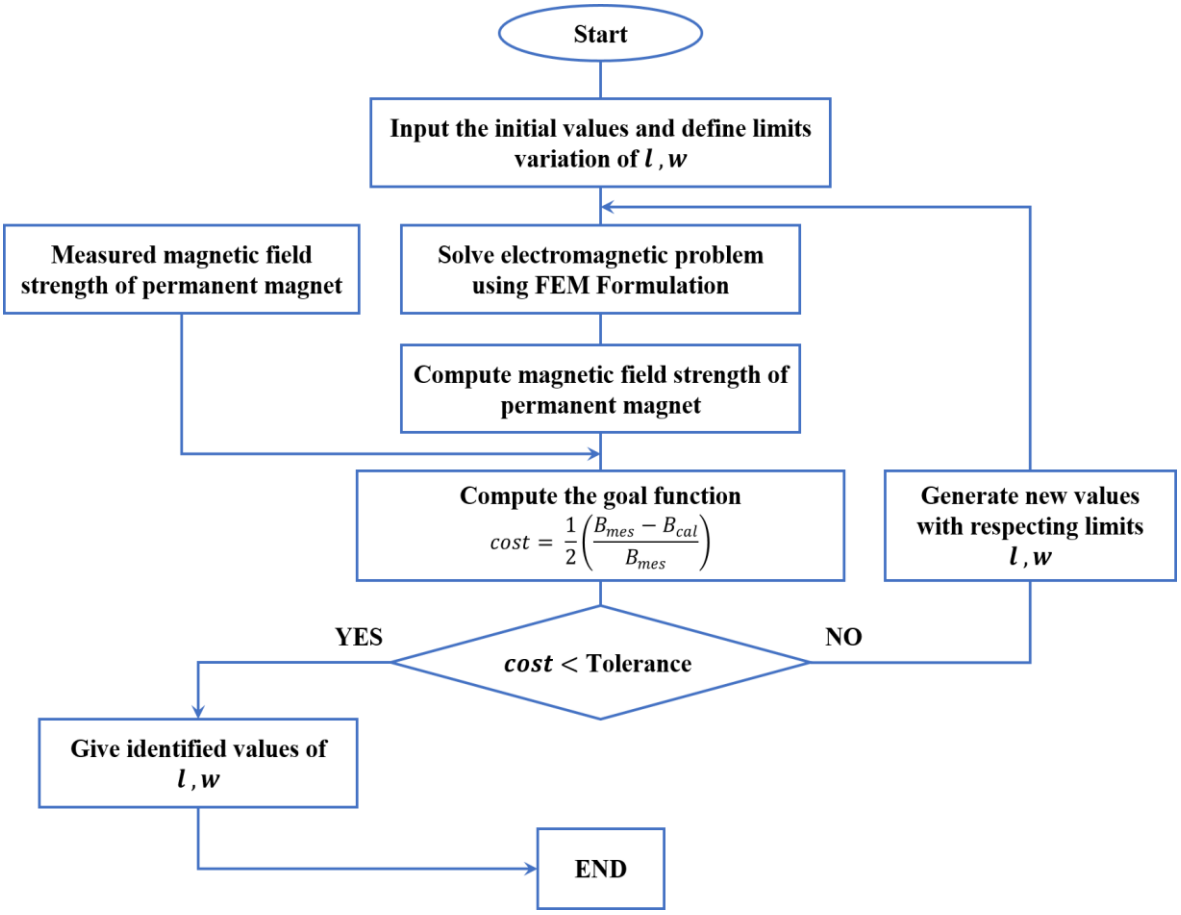

Fig.2.11 Inverse problem algorithm.

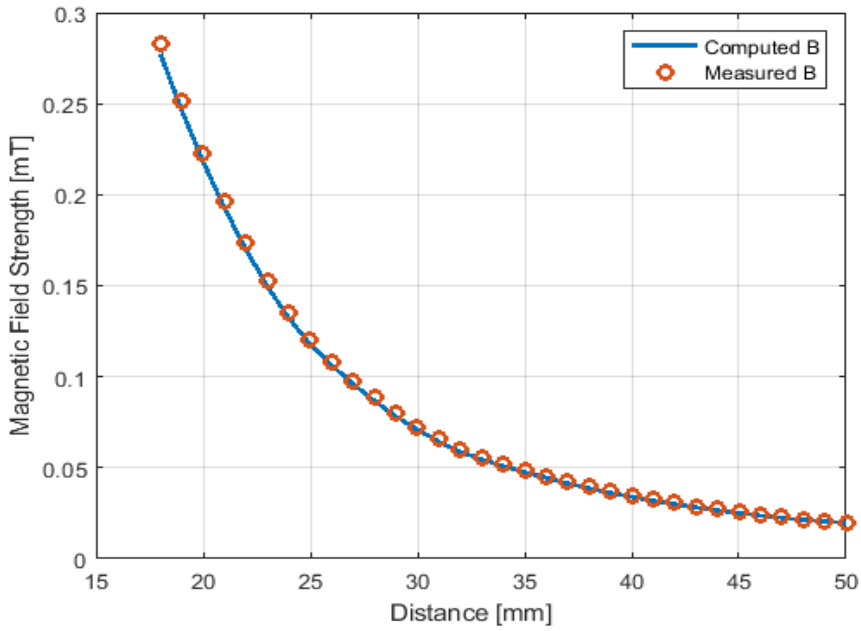

Fig.2.12. 3-D computed magnetic field strength of the permanent magnet and the measured one as a function of distance to identified the detectable area dimensions of the GMR sensor.

Figure.2 12 compares the permanent magnet's 3-D computed magnetic field strength and the measured one. The maximum error between the two results is less than 2%.

2.12. Three-D FEM model

Eddy's current NDT system comprises a differential measurement bi-GMR sensor probe inspecting a plate presenting parallelepiped cracks. The simulation of an electromagnetic system needs knowledge of all physical and geometrical characteristics in different regions.

A 3D numerical model based on the finite element method FEM is developed to simulate the EC-GMR inspection process with a differential GMR sensor and study its performance. Moreover, to validate the operation of the differential sensor for detecting cracks in a multi-layer riveted structure. The formulation is based on magnetic vector and electric scalar potential; the gauged A, A-V formulation [Helifa 16a].

The magnetic vector potential A is used in this formulation throughout the region $\Omega_n \cup \Omega_c$, and the electric scalar potential V only in Ω_c, where Ω_n, Ω_c are, the eddy current free region (such as domains containing non-conducting media and coils with known current density) and the eddy current region. The partial differential equations of! an eddy current field problem, having a unique solution according to Coulomb gauge, can be written as:

$$\nabla \times \left(\upsilon_0 \nabla \times A\right) - \nabla\left(\upsilon_0 \nabla \cdot A\right) + \sigma\left(i\omega A + \nabla V\right) = 0, in\Omega_c \tag{2.33}$$

$$\nabla \cdot \left(\sigma i\omega A + \sigma \nabla V\right) = 0, in\Omega_c \tag{2.34}$$

$$\nabla \times \left(\upsilon_0 \upsilon_r \nabla \times A\right) - \nabla\left(\upsilon_0 \upsilon_r \nabla \cdot A\right) = J_s, in\Omega_n \tag{2.35}$$

In (2.33) and (2.35), υ_0 and υ_r are, respectively, the reluctivity of vacuum and the relative reluctivity in the eddy current free region, σ is the electrical conductivity, ω is the angular frequency, and J_s is the source current density. The GMR sensors operate in a differential configuration; the probe output is expressed as given by the equation (2.36), which is implemented in ANSYS Electronics.

$$V_{out} = V_{GMR,2} - V_{GMR,1} \tag{2.36}$$

Assuming that the two GMR sensors are operating within their linear range and considering $S_{eff\,1} = S_{eff\,2}$ (for the same type of sensors), the output voltage is proportional to the local magnetic field. Hence, the output of the differential probe can be expressed using Equation (2.37).

$$V_{out} = S_{eff}\left(B_{GMR,2} - B_{GMR,1}\right) \tag{2.37}$$

Where S_{eff} is the effective sensitivity (the sensor elements are carefully matched to ensure similar sensitivity levels), $B_{GMR,1}$ and $B_{GMR,2}$ are, respectively, the magnetic field flowing through the surface of the GMR_1 sensor and the magnetic field flowing through the surface of the GMR_2 sensor.

The system study out preserved the sensor in the milieu of its linear range, and the experimental results are shown the disturbances due to the remanent magnetic fields largely attenuate to confirm the interest of this system.

2.13. Simulation Results

The simulation is performed in three steps:

In the first step, we studied adjusting the position of the GMR sensor to have the optimum sensitivity point of the probe. Therefore, we shifted the GMR sensor along the x- direction with a step of 0.01mm. Figure.2 13 shows the symmetry axes of the coil and the sensor and the GMR-Coil asymmetry (α). The curve begins with the symmetry position, the center of the excitation coil, as proven by recent research such as Romero-Arismendi and al. [Romero 20], which is the weakest sensitivity point. The results presented in Figure 2.14 proved that 2.67 mm is the best position for the maximum output voltage of the GMR sensor, which shows the optimal sensitivity compared with the center value of the probe for best detection.

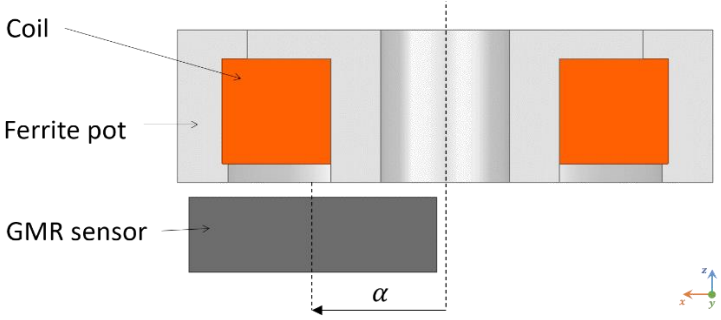

Fig 2.13 Representation of the Coil-GMR asymmetry value (α) in the GMR-based EC probe

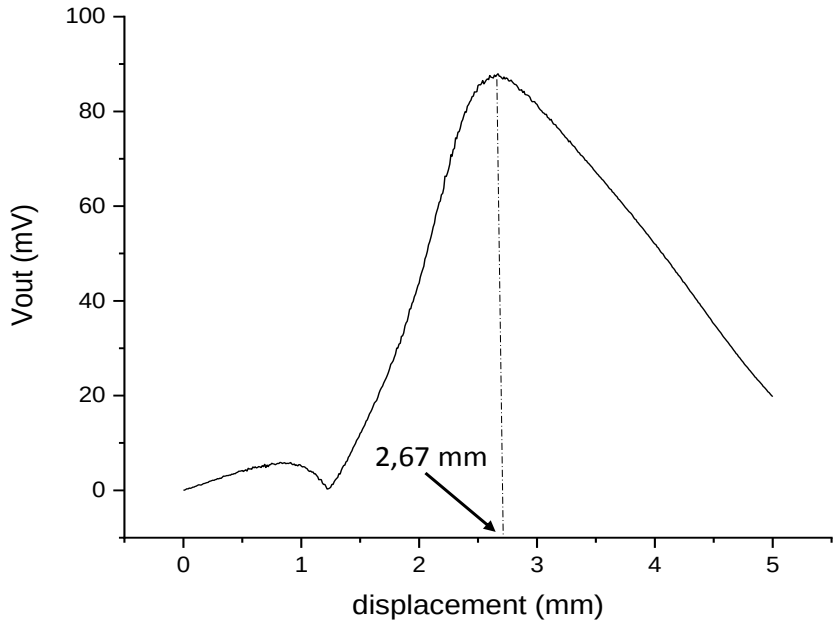

Fig 2.14 Output voltage of the GMR sensor v_s. GMR displacement.

In the second step, after determining the optimal GMR sensor location, we study the performance of the proposed differential GMR-based EC sensor. This numerical example considers the system presented in Figure 2.13. The numerical values of the modeled system parameters are given in Table 2.1. [Touil 22a]

Table 2.1 numerical values of the modeled system parameters

Element	Parameters	Values
Coil	Outer diameter (D_o)	9 mm
	Inner diameter (D_i)	4.7 mm
	Height (H)	2.2 mm
	Number of turns (N)	175
Ferrite pot core	Pot core outer diameter (D_p)	11 mm
	Core inner diameter (D_{ic})	
	Core diameter (D_c)	4.6 mm
	Crown inner diameter (D_{ir})	9.1 mm
	Inner height (H_i).	2.6 mm
	Core height (H_p)	3.2 mm
	Permeability (μ_r)	4000±25%
Aluminum plate	Conductivity (σ)	19.63×10^6 S/m
	Thickness (e)	15 mm
	Surface ($D_x \times D_y$)	80×40 mm^2
Crack	Length (L)	1 mm
	Width (W)	0.69 mm
	Depth (D)	1 mm
GMR sensor	NVE AAH002-02	
	Distance between the GMR sensors (D_g)	5.34 mm
	Typical Sensitivity	150 mV/V/mT
	Linear Range	0.06 – 0.3 mT
	Saturation	0.6 mT
	Package	SOIC8
Power source	Intensity, Frequency	8 mA, 10 kHz

The differential GMR-based eddy current sensor's output voltages are based on the FEM model. Following four conditions were studied, particularly: i) crack-free sample; 2) sample with crack 1 (length=1mm, width=1mm, depth=1mm); 2i) sample with crack 3 (length=3mm, width=3mm, depth=3mm) and iv) sample with crack 5 (length=5mm, width=5mm, depth=5mm). The GMR probe was moved along the y-axis from −10 mm to 10 mm with a lift-off of 0.1 mm.

The amplitudes of the output of the differential -GMR probe are presented in Figure 2.15. It is seen that the curve of the crack-free sample, that is, the red curve, is nearly zero, which confirms that the background signal measured in the crack-free area is null. Moreover, the output of the differential -GMR probe curves of three cracks (1, 3, and 5) show that the sensor is sensitive to flaws and confirmed that the amplitude increases with the depth of the crack to a particular value. After that, we justify the choice of the excitation coil by comparison between two symmetrical ferrite coils, one of them with ferrite pot core T6 in the same conditions of experience (the same current source passes through them). To test the Influence of the ferrite pot core on the sensitivity of the GMR measurement probe, we simulate the same investigation but with an excitation coil without a ferrite pot core, as illustrated in Figure 2.16.

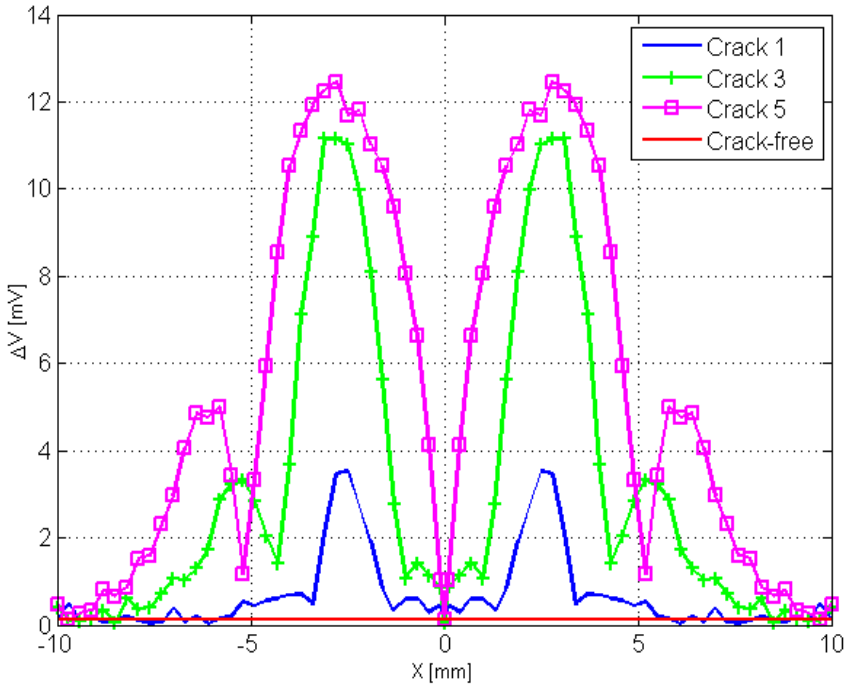

Fig 2.15 Simulation result: output voltage of the differential probe vs. probe displacement for Four different conditions: i) crack 1; 2) crack 3; 2i) crack 5 and iv) crack-free. [Touil 22a]

The numerical results are compared in the same conditions, i.e., the excitation current was set at 8 mA amplitude at 10 kHz frequency, sample with crack are length × width × depth = 5 mm × 0.69 mm × 5 mm. The scan positions during the inspection are performed for 201 positions for the first probe and the second one.

c) **b)** **a)**

Fig 2.16 Symmetrical coils: (a) up view probe with ferrite pot core; (b) up view probe without ferrite pot core; (c) down view of probes.

Figure 2.17 compares the output voltage of the differential probe with a ferrite pot core and the output voltage of the differential probe without a ferrite pot core as a displacement function. We notice that this ferrite pot core T6 of GMR- Based EC probe adds 78.16% to the sensitivity to the presence of cracks than the conventional EC sensor without a ferrite pot core. We demonstrated that the magnetic field generated by the excitation ferrite core coil in the linear range of the transfer characteristic of the AAH002-02 GMR sensor used (0.06 – 0.3 mT). Then, the magnetic field generated by the excitation coil without ferrite core out the linear range of the GMR sensor.

To give an idea about the computing time in immediate solutions. In the standard AL-Alloy with crack 1, the probe coil with ferrite pot core and the air region are discretized into 14600, 14800, 32400, 35600, and 71600 elementary tetrahedrons. The resolution time on an Intel® Xeon ® CPU E5-2620 12-core Processor 2.00 GHz workstation with 128 GByte RAM is about 2 hours and 30 minutes, which is reasonable considering the number of positions computed and the required precision. To evaluate the good magnetic response, it is unnecessary to calculate where performed with and without cracks; one scan estimates magnetic variation.

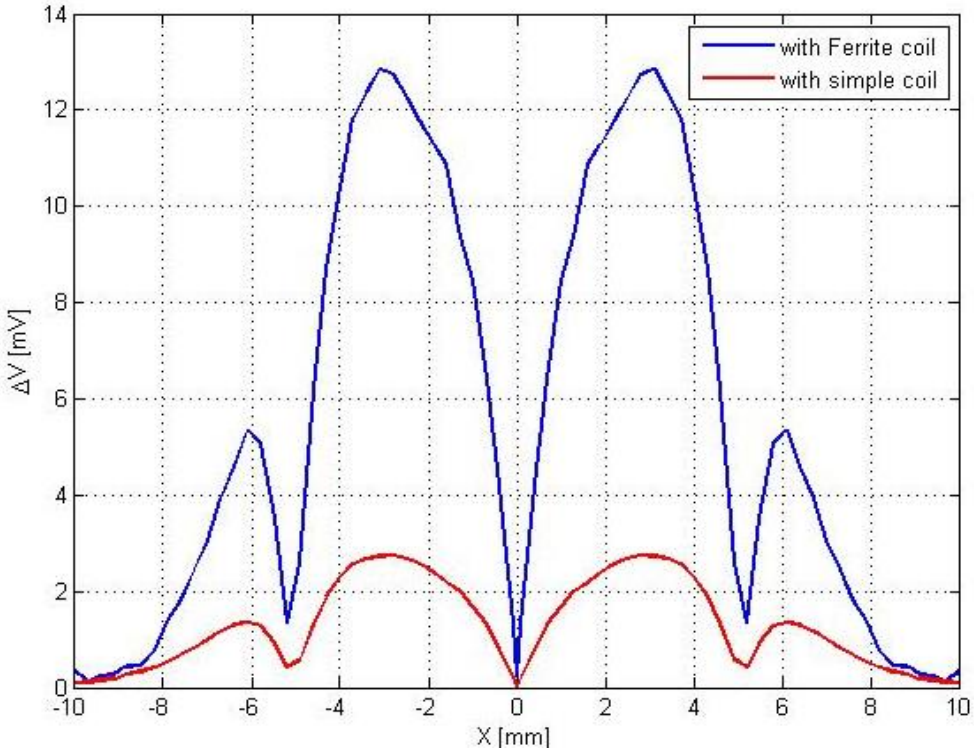

Fig 2.17 Simulation result: comparison between the output voltage results by the differential probe with a ferrite pot core and the differential probe without a ferrite pot core. [Touil 22a]

The first difficulty of that kind of calculation comes from the high numerical precision required to get the variation of the signal induced by defects. High accuracy can be obtained by mesh refinement. Still, in the case of magnetic vector potential formation, the memory required for calculation increases and rapidly exceeds the available computer RAM (128 GB).

The second complex scans the sample by moving the induce above the aluminum plate. Classically, the solution is to mesh the geometry for each position of the inducer, assemble the matrices, and solve the resulting numerical system. Nevertheless, this method leads to high CPU time calculation and often generates high numerical noise due to mesh variability. Another advanced solution uses the perturbation technique for the finite element method. The main advantage of this elegant method is to avoid meshing. The perturbation approach for modeling nondestructive testing problems seems efficient, especially for complex inducers, such as high permeability flux concentrators.

A butter resolution requires a skinny mesh of the studied system, this last, which increases the simulation time. For this reason, the refinement concerns only the sensitive zones, such as the sensor and neighboring space of crack. The mesh depicts in Figure 2.18.

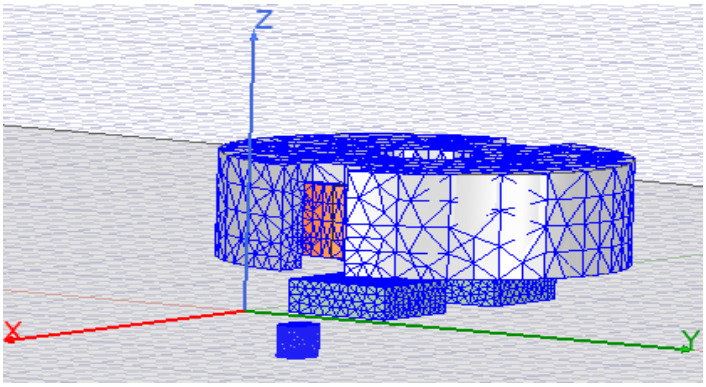

Fig 2.18 3D finite elements mesh.

2.14. Conclusion

In this chapter, we present the design and implementation of a high-sensitivity Eddy Current (EC) sensor based on giant magnetoresistance (GMR) for inspecting aluminum samples with machined cracks. A significant contribution of our work is to show that one can employ differential measurements from asymmetric differential GMR sensors to eliminate the background signal.

- The 3-D model uses to compute the magnetic field strength of the permanent magnet to evaluate detectable area dimensions of the GMR AAH002 02 sensor, an experimental prototype unit consisting of the GMR sensor proposed and the permanent magnet as a distance function (Axial Magnet), and microcontroller interface. The magnetic field B change the output voltage on the GMR sensor. The inverse problem goal function is minimized using the particle swarm optimization (PSO) algorithm to evaluate the detectable area dimensions according to the measurement of the magnetic field strength at the GMR sensor's location.
- The 3-D numerical model is used to adjust the position of the GMR sensors-excitation coil at the optimal sensitivity point of the probe; it is found that it is about 2.67mm from the center of the excitation coil.
- The comparison between the 3-D computed magnetic field strength of the permanent magnet and the measured one show a significant concordance. The maximum error between the two results is less than 2%.

CHAPTER 3

GMR probe construction: Experimentation and prototyping

Contents

3.1. Introduction

In this chapter, we present the results obtained during the practical tests of the prototype carried out at the Laboratory of Physics of Materials (LPM) at Laghouat University.

Firstly, we propose new design identification of a mono-element giant magneto-resistance (GMR) probe and a new concept of a differential GMR measurement probe. Then, we show the geometric, electrical, and physical characteristics of GMR and excitation coil components. In addition, we present the different realized electronic boards to supply the sensor with a two-phase voltage source and to multiplex and pre-amplify the signals. The new concept of a differential GMR eddy current probe, excited by external sinusoidal excitation currents from generator multiplexer (MUX) with internal source Lock-in Amplifier, in order to Investigate double signal and mixing signals GMR and internal signal for best results. In addition, internal continue excitation current source from Lock-in Amplifier to GMR sensors.

After that, we present the devices (Lock-in Amplifier) and their performance. The material (Al Alloy) is inspected, and the samples (with machining defects) are described.

Finally, we present the measurement strategy of the realized prototype with their experimental results and the validation of simulation results.

3.2. GMR probe: conception and construction

3.2.1. Mono-element magnetoresistance probe

In this part, we present the new proposed eddy current sensor that we produced in our Laboratory LPM; it is shown in Figure (3.1).

The mono-element GMR probe is composed of a coil mounted on a ferrite pot and a giant magnetoresistance sensor. We chose GMR AAH004 00E as a receptor because of the high sensitivity and the small size and a ferrite coil because the emitting magnetic field produced increases in the middle. The characteristics of the excitation coil manufactured by SCIENSORIA are given in (see Table 3.1).

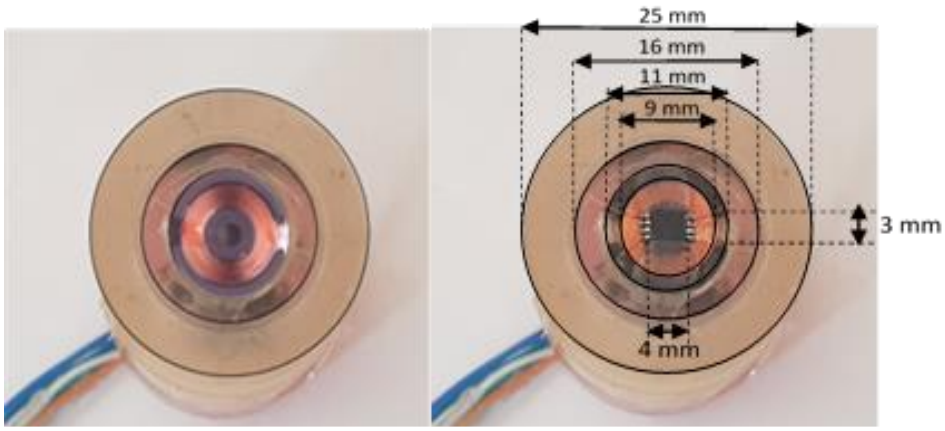

Fig.3.1. Inductive and giant magnetoresistance probes.

Table 3.1 Characteristics of the excitation coil

Designation	Dimension Coil	Observations
CAP3 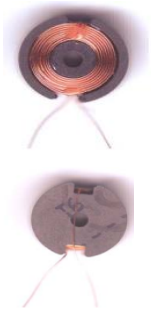	Inside radius: 4.7 mm Outside radius: 9 mm Length of coil: 2.2 mm Number of turns: 175 Number of layers: 14 Diameter of wire: 0.14 mm Dimension Pot en ferrite : T6 Ferrite pot size Material: T6 Core diameter:4.6 mm Internal ring diameter: 9.1 mm Internal height:2.5 mm Permeability : μ_r=4000±25%	A flat coil. Mounted on a ferrite pot.

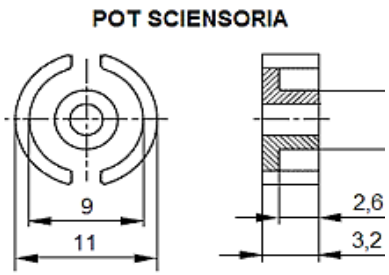

3.2.1.1. Giant magnetoresistance sensor characteristics

A giant magnetoresistance sensor of the type AAH004-00 manufactured by NVE Corporation is used according to the [catalog 21]; their characteristics are presented in (Table 3.2)

Table 3.2 Characteristics of the Giant Magnetoresistance

Designation	Dimension Coil	Observations
GMR **NVE** **AAH004-00** 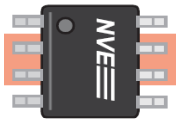	Saturation: 1.5 mT= 15 Oe Sensitivity: 32-48 V/T/V Linear Range: 0.15 et 0.75 mT Resistance: 2K ± 20% (ohms) Power supply: 9 V Dimension of GMR sensor: 3 × 1.5 × 1 mm Package: MSOP8	Giant magnetoresistance NVEAAH004 Forfait (Package) MSOP Taille (Die sizeμm) 411× 1458
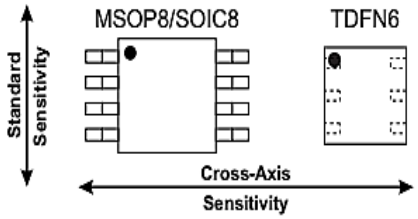		

Figure 3.2 depicts non-volatile electronics that produce the internal configuration of the giant magnetoresistance sensor AAH004-00. The GMR sensor consists of four resistors in a Wheatstone bridge. A material layer connects four GMR magnetically with high magnetic permeability.

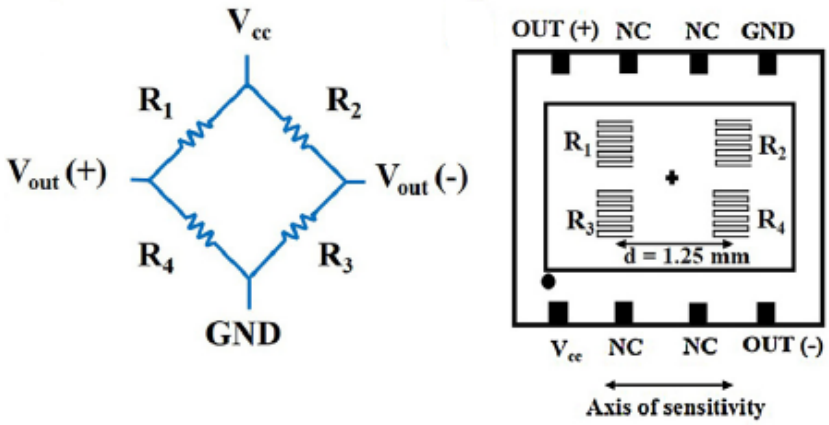

Fig.3.2. Giant magneto-resistor bridge sensor [catalog 21].

The output voltage equation of the giant magnetoresistance used [catalog 21]:

$$\Delta U = S_{eff} \cdot B \tag{3.8}$$

Where the effective sensitivity, the multiply of the medium sensitivity, and the supply voltage. For an AAH004-00E GMR sensor, S_m=32-48 (mV/V/mT), and a supply voltage V_s = 9 (V), depicted in table 3.2. [Catalog 21] *B* magnetic flux density ‘‘flowing’’ through the surface of the giant magnetoresistance sensor.

3.2.1.2. Experimental setup of the eddy current system

Figure.3.3 shows the experimental setup, an Aluminum plate with cracks of different depths and a giant magnetoresistance probe. In this experiment, The GMR probe is scanned over the surface of the Aluminum plates in the direction of the giant magnetoresistance sensing axis perpendicular to the sample because it is the region where the maximum perturbation of the x component of the magnetic field density (B_x) occurs.

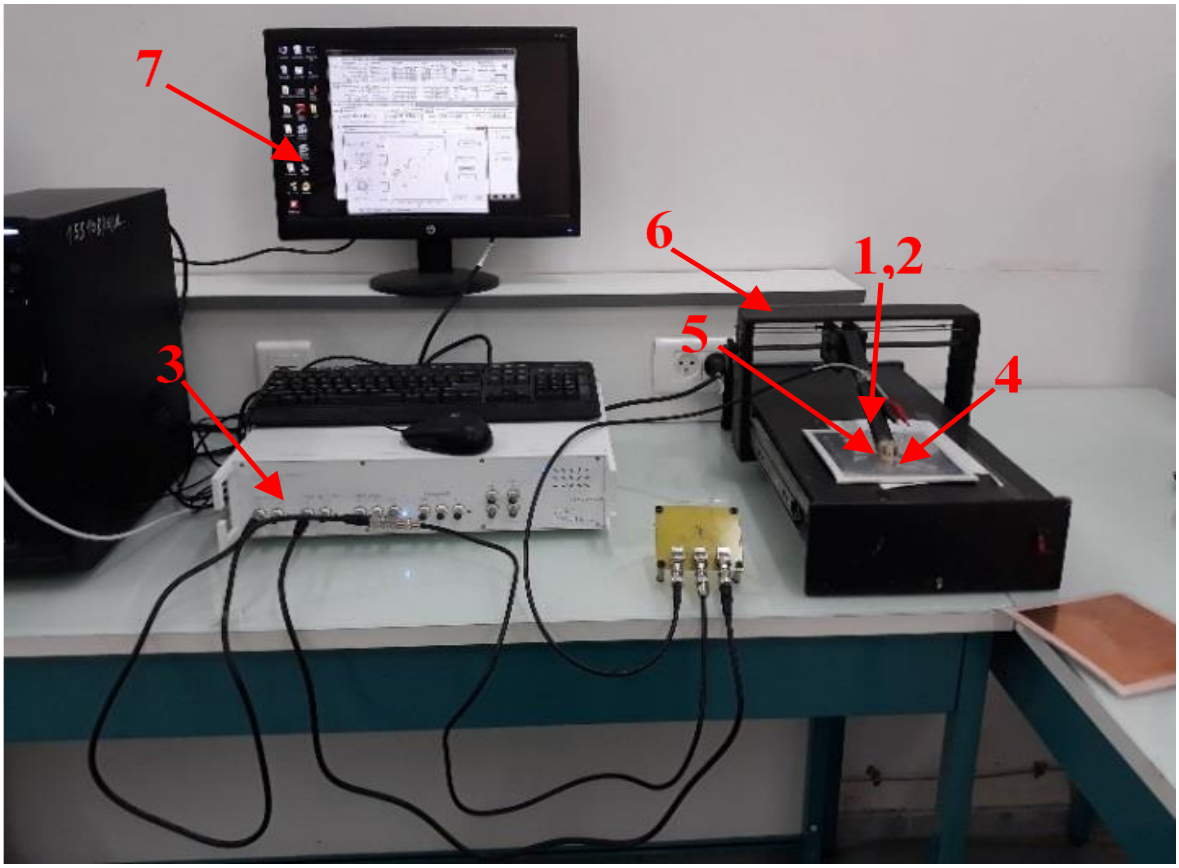

Fig 3.3 Measuring System.

Table 3.3 Composants du montage expérimental

	Sensor displacement System
1	Sensor (Ferrite Coil)
2	Sensor (Giant Magnetoresistance),
3	Lock-in Amplifier HF2LI
4	Test Sample
5	Cracking Opening
6	Sensor Displacement System
7	Pc-Interface.

The set of experiment equipment:

- A magnetic probe composed of a magneto-resistance GMR AAH004 00 manufactured NVE receiving sensor and an excitation coil with a ferrite core.
- A robotic table with two stepper motors is controlled by (Arduino) for the movement of the sensor.
- The test sample is Aluminum Alloy.

- A Lock-in Amplifier (synchronous detection amplifier) measures the voltage variation across the sensor.
- A PC to control the Lock-in Amplifier.
- The whole of the material used is presented in figure 3.3 and is detailed in table 3.3.

3.1.1. Synchronous detection Amplifier "HF2LI Lock-in Amplifier"

The synchronous amplifier HF2LI (Fig.3.4) detection is used to process the signal. Their signal has very low amplitude and high frequency and is drowned in measurement noise which is low frequency (see Fig.3.5). The detection used to determine the amplitude of the signal, although it is minimal. The amplitude of this signal can be of the order of *nano volts* and can be detected by this method. It is isolated from all undesired frequencies and phases to recover this signal. So noise cannot affect the measurement. For isolation, it is necessary to have a reference frequency. A synchronous detection amplifier or "Lock-in amplifier" is used to extract the desired amplitude to realize this measurement.

Fig.3.4 HF2LI Lock-in Amplifier.

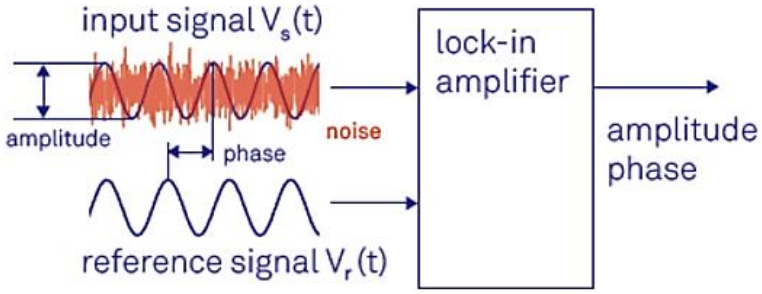

Fig.3.5 The process for measuring the amplitude and phase of a signal by a synchronous detection amplifier.

3.2. General Principle of synchronous detection

3.2.1. Dual phase demodulation

In a typical experiment, the device under test (DUT) is excited by a sinusoidal signal, as shown in Figure (3.6 (a)). The response of the device V_s (t) and the reference signal V_r (t) uses by the synchronous sense amplifier to determine the amplitude V and the phase θ, and this is achieved using a dual-phase demodulation circuit, as shown in Figure (3.6 (b)). The input signal divides and multiplies separately with the reference signal and a 90 ° phase-shifted.

The output mixers are passed through configurable low pass filters resulting in both X and Y outputs called in-phase and quadrature components. The amplitude A_s and the phase θ are easily derived from X and Y by transforming Cartesian coordinates into polar coordinates using the relation:

$$\frac{A_s}{\sqrt{2}} = \sqrt{X^2 + Y^2} \tag{3.1}$$

$$\theta = \alpha \tan 2(Y, X) \tag{3.2}$$

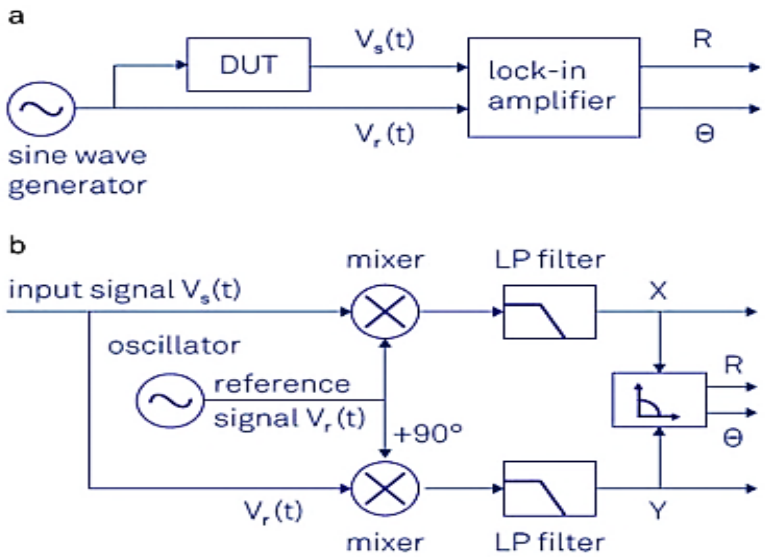

Fig.3.6 (a) Basic measurement configuration incorporating a synchronous detection amplifier. (b) Mixing and low pass filtering performed by the synchronous detection amplifier.

3.2.2. Mixing of signals in the temporal domain

Complex numbers provide an elegant mathematical formalism for calculating the demodulation process. We use the elementary trigonometric law to rewrite the input signal V_s (t), as the sum of two vectors in the complex plane:

$$V_S(t) = \frac{A_S}{2} e^{+j(w_S t+\theta)} + \frac{A_S}{2} e^{+j(w_S t+\theta)} = A_S . \cos(w_S t + \theta) \tag{3.3}$$

The dual-phase mixer is expressed mathematically as a multiplication of the input signal with the complex reference signal:

$$V_r(t) = \sqrt{2}\, e^{+j(w_r t)} = \sqrt{2}\cos(w_r t) - j\sqrt{2}\sin(w_r t) \tag{3.4}$$

The complex signal after multiplication is given by:

$$V(t) = X(t) + jY(t) = V_S(t).V_r(t) = \frac{A_S}{2}[e^{+j((w_S - w_r)t+\theta)} + e^{-j((w_S - w_r)t+\theta)}] \tag{3.5}$$

The complex signal after multiplication gives by the following filtering and mathematically expressed. As an average of the moving vectors in time. The filtering overrides the term fast rotation at $|w_s - w_r|$ by defining $\langle \exp[-j((w_s - w_r)t + j\theta)] \rangle = 0.$

The signal after demodulation in the case where the frequencies are equal $W_s = W_r$ becomes:

$$V(t) = \frac{A_S}{2} e^{j\theta} \tag{3.6}$$

Equation (3.6) is the demodulated signal and the main output of the synchronous detection amplifier: with the absolute value $\|V\| = A_s/\sqrt{2}$ given as the effective value of the signal and its argument $\arg(V) = \theta$ given by phase shift of the input signal concerning that reference. The real and imaginary parts of the demodulated signal $V(t)$ are the components in phase X and quadrature Y. They obtained using Euler's formula:

$$\begin{cases} X = \mathrm{Re}(V) = \dfrac{A_s}{\sqrt{2}}\cos\theta \\ Y = \mathrm{Im}(V) = \dfrac{A_s}{\sqrt{2}}\sin\theta \end{cases} \tag{3.7}$$

Figure 3.7 depicts the Schematization of the measurement system explained in the Block diagram of the experimental setup for the Eddy current measurements. A lock-in amplifier HF2LI is used to improve the signal-to-noise ratio. A sinusoidal voltage signal is selected with a Lock-in amplifier of 1 V_{pp} and different frequencies. This signal is sent to the excitation coil and thus generates an AC-magnetic field.

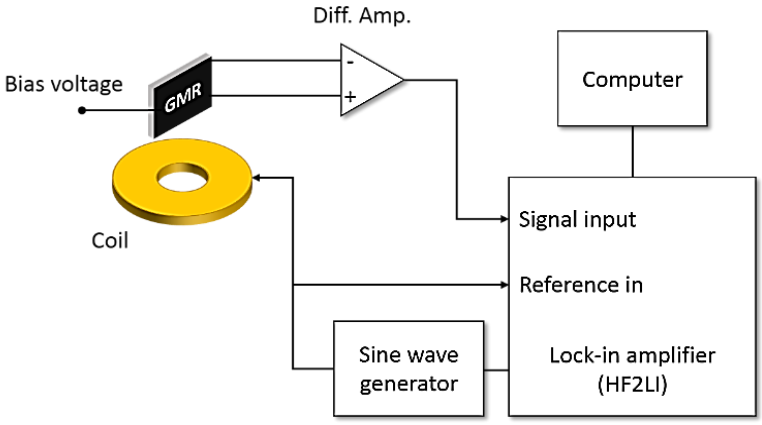

Fig.3.7 Schematization of the measurement system.

The component of the magnetic field induced by the eddy current in the Aluminium Alloy testing sample is measured by the sensor located in the center of the coil. The resulting signals are then connected to the lock-in amplifier's inputs. The internal reference frequency is f = 10 kHz; this instrumentation determines the amplitude.

3.1.1.1. Aluminium alloy sample

In this study, an Aluminium alloy sample is fabricated by laser devices µScan 6.5; the sample size is shown in Figure 3.8 (165×80 mm^3 testing by profilometer), conductivity σ = 35; 59 MS / m. Ten surface flaws extend from the edges of the sample (see Table 3.4).

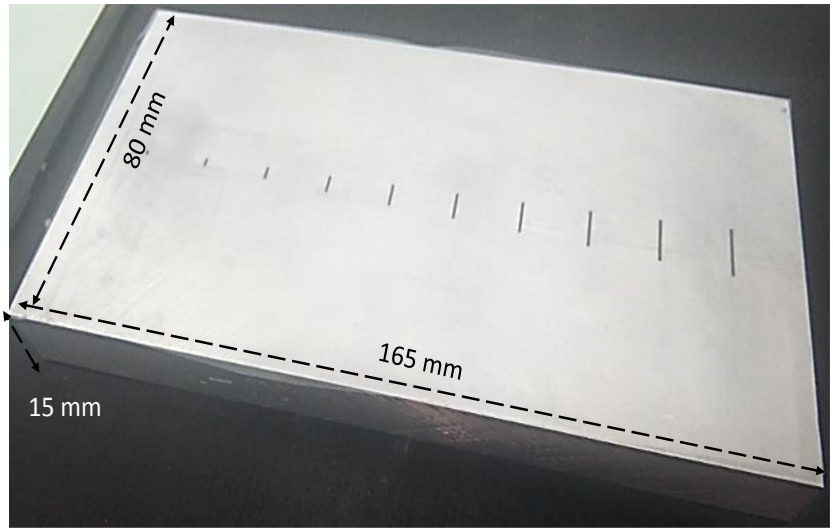

Fig.3.8 Standard Aluminum Alloy with machined flaws.

Table 3.4 Numerical Values of Dimensions of the Cracks.

Cracks	Length	Width	Depth
1	1.00 mm	0.67 mm	1.00 mm
2	2.00 mm	0.68 mm	2.00 mm
3	3.04 mm	0.68 mm	3.00 mm
4	4.03 mm	0.69 mm	4.00 mm
5	4.95 mm	0.65 mm	5.00 mm
6	5.43 mm	0.62 mm	6.00 mm
7	6.05 mm	0.57 mm	7.00 mm
8	7.65 mm	0.47 mm	8.00 mm
9	8,18 mm	0.61 mm	9.00 mm
10	8.94 mm	0.55 mm	10.00 mm

3.2.2.1. Experimental results

The general procedure is to scan the area, including the crack, with a giant magneto-resistance probe, the measurement depicted in Figure.3.9.

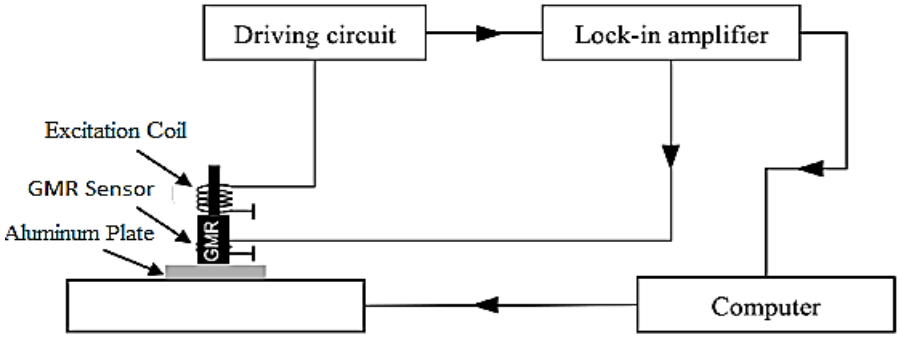

Fig.3.9. Schematic of the experimental setup for the eddy current testing system with giant magnetoresistance probe.

The sensor has an active area of about 100 by 200 mm in the middle of the layout [Dogaru 01], and the lift-off of the active zone of the giant magnetoresistance sensor is approximately 0.5 mm [Kim 10]. The same excitation coil is used for the exact measurement. The results include the variations of the tension records; it is valuable information about crack characterization. Figure.3.10 depicts the scan tests performed to evaluate the sample. One surface cracks its length

is about 14 mm, and the width and depth of 1 mm, and 5 mm. respectively; it is machined in an Aluminum plate with a thickness of 20 mm.

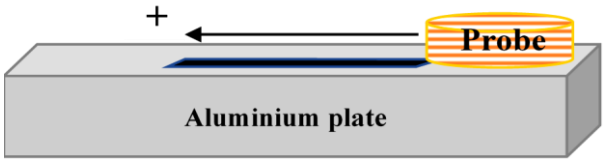

Fig.3.10 Schematic of the scanning tests

An increase in the output voltage of the giant magneto-resistance and inductive probes is observed when the sensor moves on the top of the crack; after further movement, the output voltage sensor returns to the previous value. The giant magneto-resistance sensor amplitude is increased compared with the inductive sensor, which confirms the high sensitivity of the Giant magneto-resistance probe (see figure 3.11).

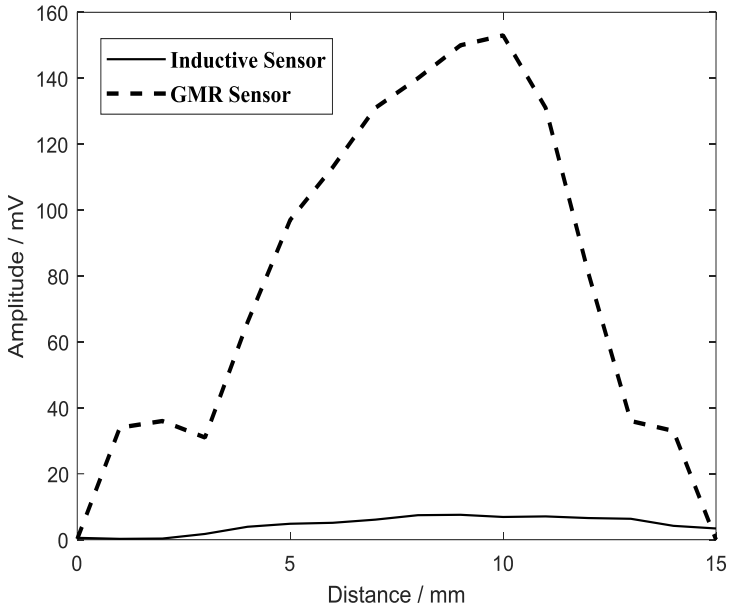

Fig.3.11 Giant magnetoresistance and Inductive output voltage

We repeated the same experiment but chose a scanning excitation frequency range of 20 kHz–160 kHz. We compare the signal amplitudes of the flaws. The frequency scanning results for the crack shows in Fig.3.12. We chose the same scanning excitation range to determine the optimum excitation frequency of the eddy current testing system with the giant magnetoresistance sensor. The results show in Fig.3.13. [Touil 22b,Touil 19]

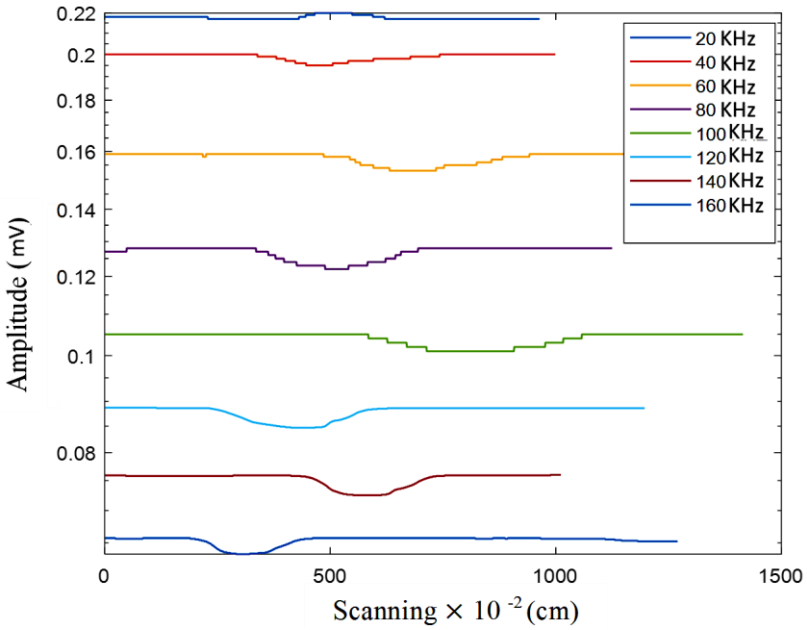

Fig 3.12 Results of the frequency scanning experiment for the Eddy current testing system with inductive sensor

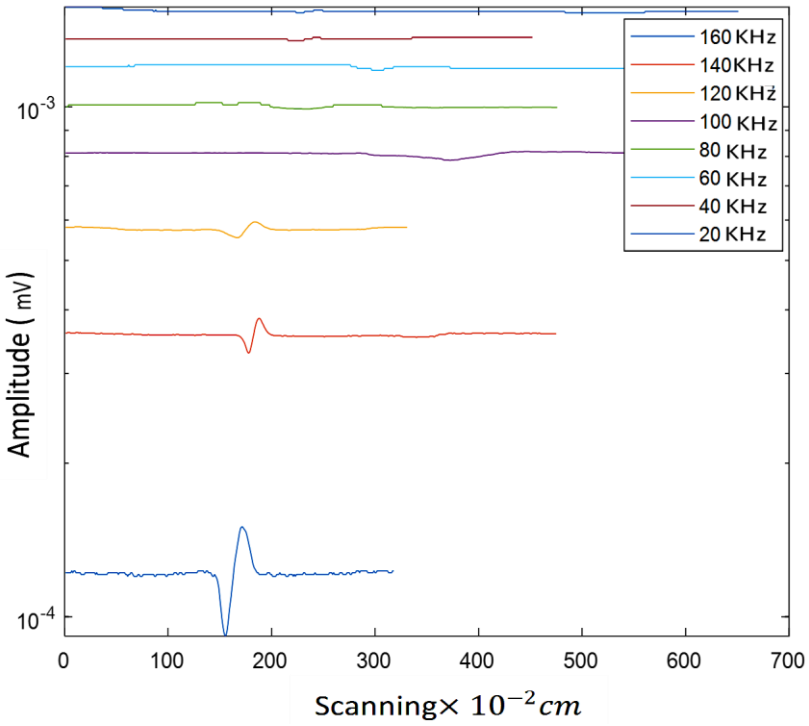

Fig 3.13 Results of the frequency scanning experiment for the Eddy current testing system with giant magnetoresistance sensor. [Touil 22b]

The results reveal that as the scan frequency change, the signal contrast between the flaw and non-flaw positions gradually change and tends toward a stable level if the sample is without cracks

with no significant output variation measure. Figure 3.12 shows that the inductive probe includes high sensitivity when we apply a very high frequency close to the resonance frequency.

Besides, the giant magnetoresistance probe keeps high sensitivity when we use weak frequencies; it is less sensitive to high frequencies.

Figure 3.14 shows typical giant magnetoresistance output signals of cracks at 20 kHz frequency when the scanning tests are performed along with the sample. [Touil 22b]

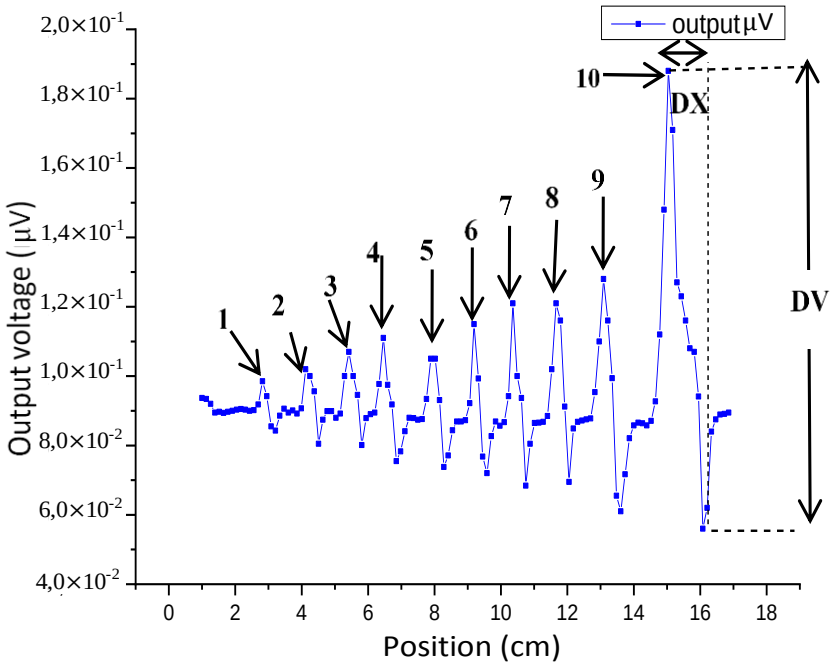

Fig. 14 Typical giant magnetoresistance voltage of cracks for the 10 nominal depths which are d=1,2,3,4,5,6,7,8,9,10 mm for each nominal width: w1=0.67 mm, w2=0.68 mm, w3=0.68 mm, w4=0.69 mm, w5=0.65 mm, w6=0.62 mm, w7=0.57 mm, w8=0.47 mm, w9=0.61 mm, w10=0.55 mm.

3.2.3. Differential magnetoresistance probe

In this part, we present the second new proposed eddy current sensor in our Laboratory LPM; it is shown in Figure (3.15).

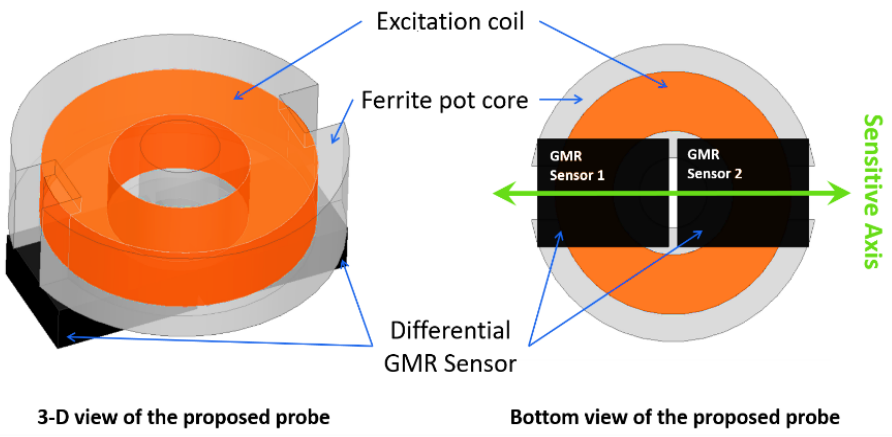

Fig.3.15 Differential GMR Probe-Design

Section 2 presents simulation results that demonstrate the feasibility of the proposed probe. A prototype differential probe, data acquisition, and motion control system are developed and tested to demonstrate the proof of concept. We use the prototype probe to build the prototype probe with the GMR sensor model AAH002-02E from Nonvolatile Electronics (NVE). AAH002-02E is extremely sensitive to the magnetic field (typically 150mV/V/mT) [catalog 21]. The measured range of the sensor is about 0.06 - 0.3 mT. The sensor can work in the frequency range from DC to 1MHz. Moreover, we utilized an excitation coil, which SCIENSORIA Sarl supplied.

3.2.3.1. Probe development (Geometric, electrical and physical characterization)

The characteristics of this probe are summarized as follows: an emitting coil with a ferrite pot. The coil characteristics the given in chapter 2. Table 2.3.

The choice of these flat coils linked to the problem being treated which consists in characterizing an emerging crack. For this purpose, it is not necessary to have strong fields, such as those of cylindrical coils with a ferrite pot and a GMR NVEAAH002 magnetic sensor. All the characteristics of the giant magnetoresistance given in chapter 2. Table 2.3.

The GMR sensor sits centrally on the bottom of the coil and with its sensitive axis oriented horizontally, parallel to the specimen sample as shown in Figure 2.1. Thus the excitation field on the axis of the coil, being perpendicular to the detection axis of the GMR, is not detected by the sensor. The positioning of the sensor has been monitored with an oscilloscope to minimize the excitation field detected. Magnetic sensors have a small active area that they approach the magnetic field point sensors allowing good spatial resolution [catalog 21].

Magnetic sensors have a small active area that approaches the magnetic field point sensors allowing good spatial resolution [catalog 21]. The GMR sensor sits centrally on the bottom of the coil and with its sensitive axis oriented horizontally, parallel to the specimen sample, as shown in Figure 2.1. The positioning of the sensor is monitored with an oscilloscope to minimize the excitation field detected.

Eddy currents (EC) are induced in the plate and have circular symmetry in the aluminum plate without defect, so no effect is produced on the GMR sensor output. The presence of a defect, such as a crack, acts as a high resistance barrier and disrupts EC paths. This disturbance manifests in the magnetic flux density picked by the sensor.

Generally, the diameter of the coil should be comparable to the thickness of the test object and similar to the expected defect length. Compact probes have higher sensitivity and resolution. However, they prevent a faster inspection of the components. A minimal coil area is also acquired to ensure an appropriate current density.

A stand with the spool is designed to achieve a more stable position with constant lift-off during automatic scanning, representing one of the most significant errors affecting the measured data. The electrical characteristics of excitation coils are measured at 10 kHz (see Table 3.5).

Table 3.5 Numerical values of electrical characteristics of a coil measured at 10 KHz.

Parameters	Ferrite pot core coil	Simple coil
Voltage (V)	0.4386 V	0.09684 V
Current (I)	8 mA	8 mA
Impedance (Z)	54.5968 Ohm	12.112 Ohm
Magnetic field (B)	0.3 mT	0.07 mT
Output voltage of GMR sensor 1&2 [a]	45 mV	10.1766 mV

[a] AAH002-02: linear range (22.5 mV - 45 mV) = (0.15 mT - 0.3 mT).

3.2.3.2. Experimental measures

In this section, we present the practical results obtained and the measuring system

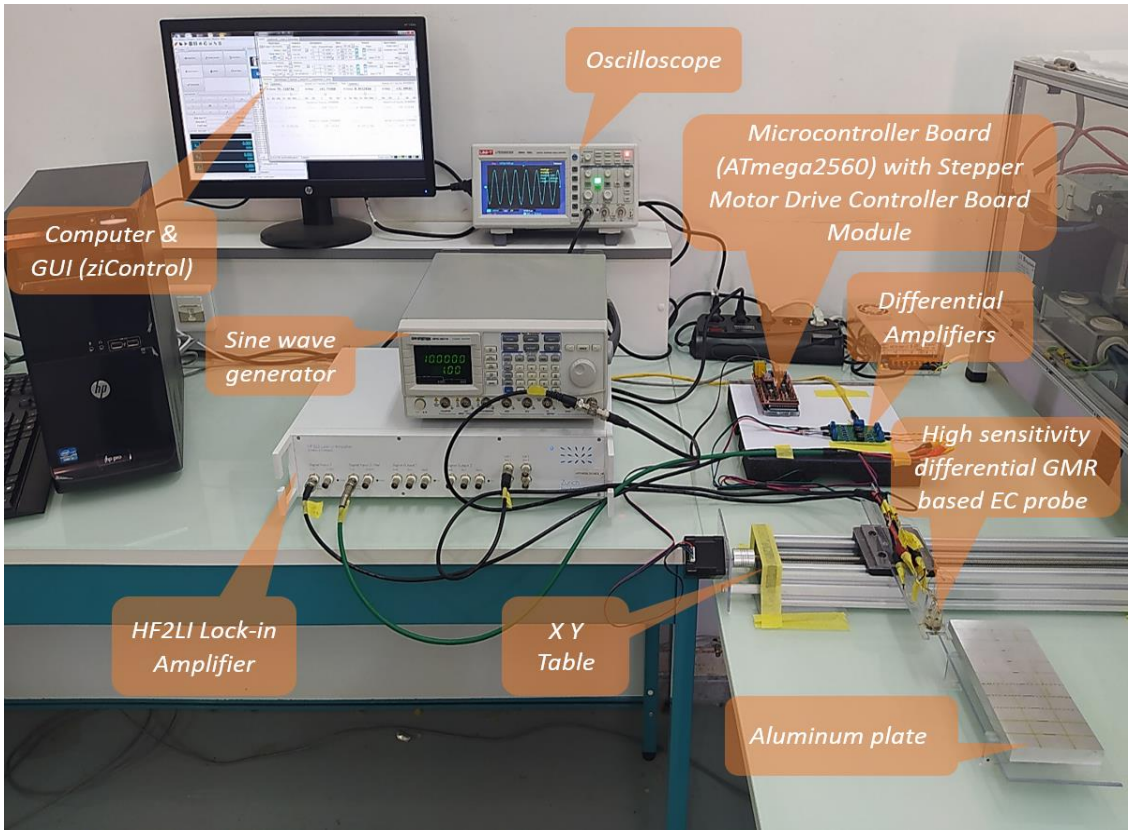

Fig.3.16. Experiment workbench.

All the equipment used in this experiment is depicted in Fig 3.16; it is composed of the following:

- Synchronous detection amplifier (Lock-in Amplifier HF2LI);
- Differential bi-GMR sensor(A magnetic probe made up of a GMR AAH002 00 manufacture magnetoresistance NVE receiving sensor and an excitation coil with a ferrite core)
- Controller (zi-Control);
- Oscilloscope;
- A robotic table with two stepper motors driven by Arduino for moving the sensor;
- Power supply board (two-phase voltage source);
- Multiplexing and preamplification card;
- Test samples;

3.2.3.3. Electronic card developed

We realize three cards shown in Fig 3.17. The first has the function of supplying our sensor with a two-phase sinusoidal current source, and the second and the third are used for multiplexing and pre-amplification.

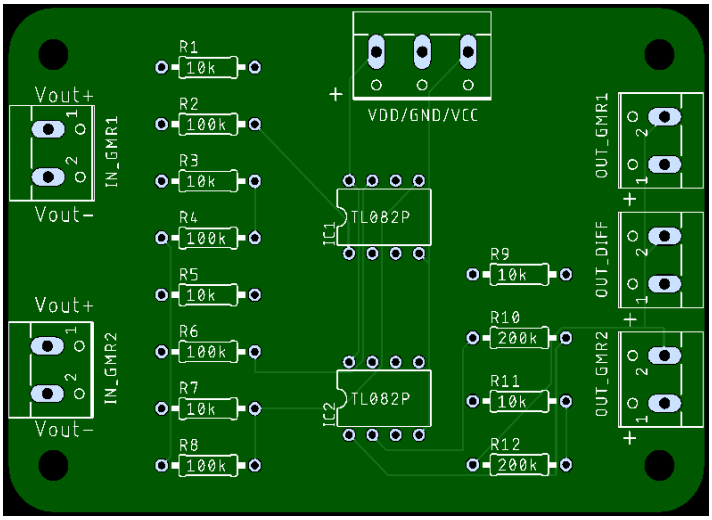

Fig..3.17 Preamplification card.

3.2.3.4. Measurement strategy

The diagram of the experiment setup is shown in Figure 3.18. The excitation signal generates by a signal generator (GW INSTEK GFG-3015), which has one output channel. This signal generator is connected to the excitation coil via a coaxial cable, whose exciting frequency is set to 10 kHz. The AAH002-02E GMR sensors are supplied with a 1 V constant voltage of a lock-in amplifier auxiliary signal. For this voltage, the current through each sensor was about 0.5 mA (the internal resistance for each sensor is 2kΩ ± 20%). A dual instrumentation amplifier is used to amplify the output signals from GMR sensors; each channel is set to a gain of 10. The resulting signal is further amplified by another amplifier, set to a gain of 20. The resulting signals are then connected to the lock-in amplifier's inputs, and the internal reference frequency is defined as f_{eff}= 2× 10 kHz. Since two almost identical AAH002-02E GMR sensors are used, a double differential measurement system the advantage and precision compared with a single differential measurement setup is further amplified.

A personal computer (PC) uses as the central data acquisition controller. It communicates with an Arduino Microcontroller Unit (AMU) through a USB cable. The AMU generates a driving signal for a step motor, which drives the probe to move on top of the tested plate. The HF2LI lock-in amplifier is used to obtain the baseband signals. The HF2LI lock-in amplifier outputs are sampled by 14 bits, 210 MSa/s Analog to Digital Converter (ADC), and acquired by the computer through a USB cable.

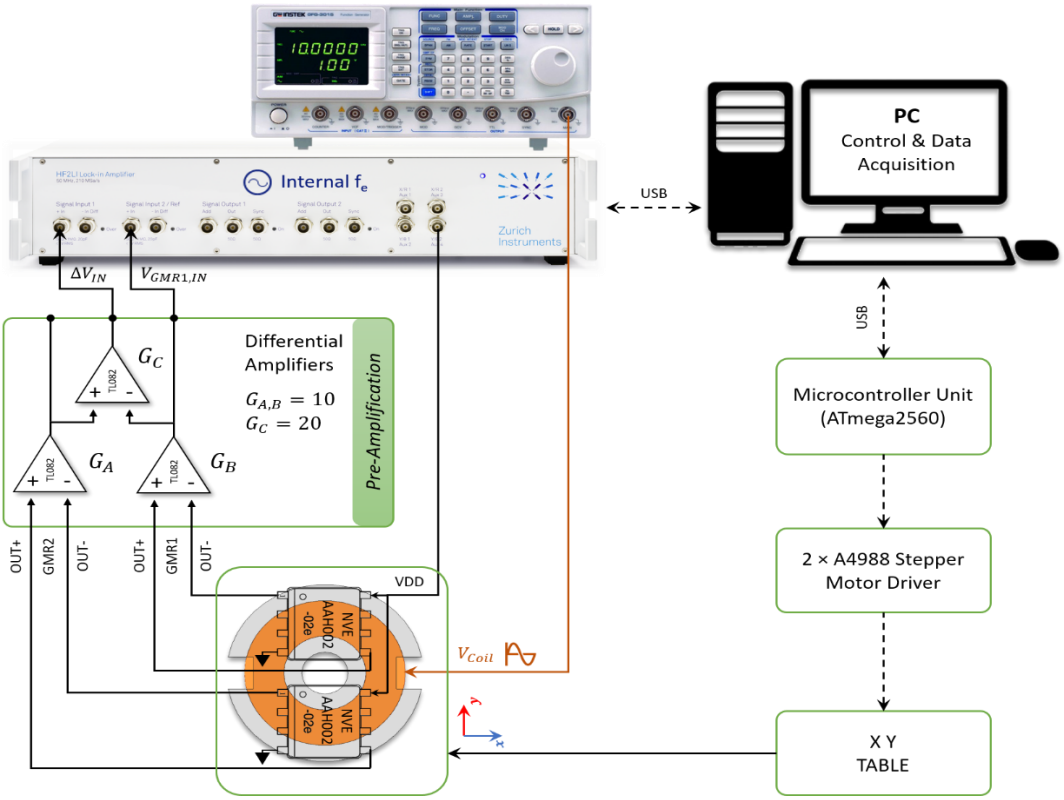

Fig.3.18. Schematic diagram of the experimental setup.

3.2.3.5. Experimental results

Figure 3.19 illustrates the experimental measurements of the output voltage of the differential probe as a function of displacement of the probe for the first five cracks (1, 2, 3, 4, and 5). Thus, the crack length and depth effect on the EC signal is apparent. Therefore, one can conclude that the EC signal strongly depends on the crack length and depth for thin cracks.

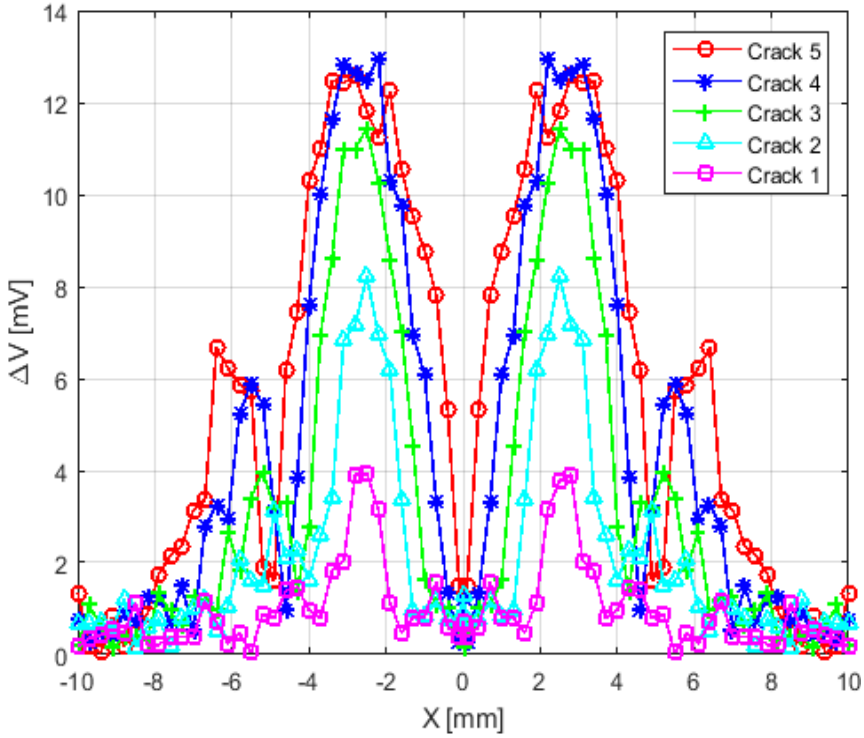

Fig.3.19. Output voltage of the differential probe vs. probe displacement for cracks (1, 2, 3, 4 and 5).

Fig.3.20 shows the experimental measurements of the output voltage of the differential probe as a function of the probe displacement for the first five cracks (6, 7, 8, 9, and 10). Thus, the crack length and depth effect on the EC signal is also apparent. On the other hand, we notice that the signal amplitudes of the output voltages of the differential probe as a function of displacement of the probe decrease, whereas the crack length and depth increase. We must note here that this phenomenon is not related to skin depth. It has to do with the distance between the two GMR sensors.

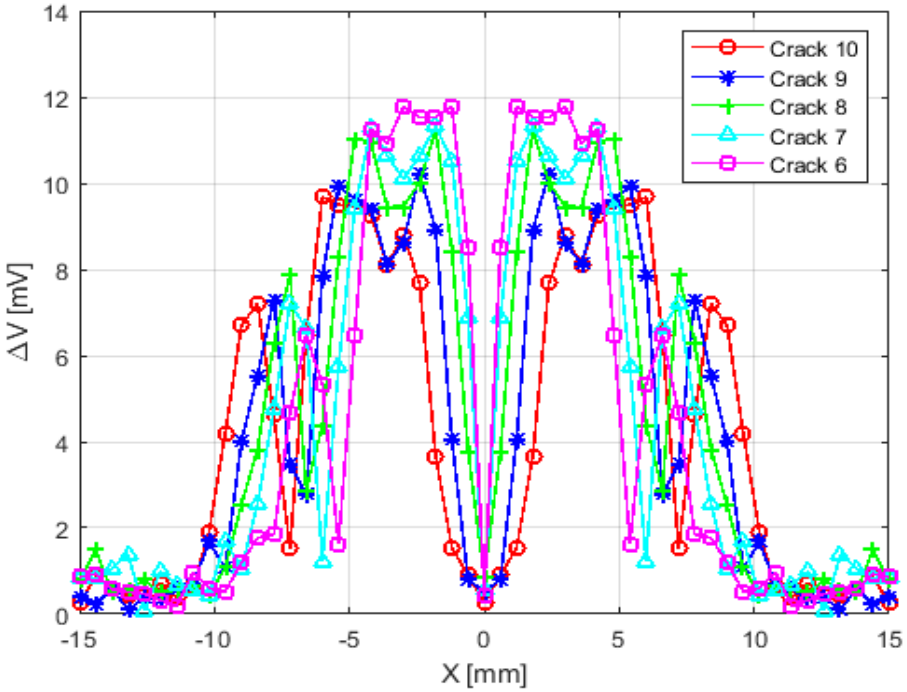

Fig.3.20 Output voltage of the differential probe vs. probe displacement for cracks (6, 7, 8, 9 and 10).

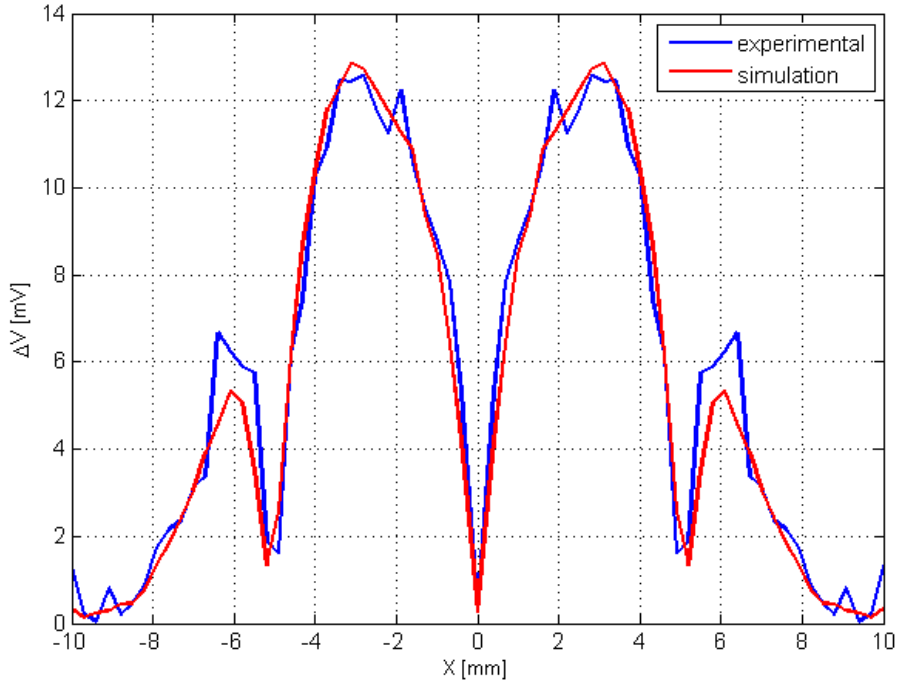

Fig.3.21. Measured and computed output voltage of the differential probe vs. probe displacement in the case of the sample with crack 5.

These results show that the probe is sensitive to cracks of different dimensions.

To check the validity of all systems, we compare the calculated and measured values of the output voltage of the differential GMR-based EC probe for a frequency of 10 kHz. Fig.3.21 shows

a comparison between the computed output voltage of the differential probe as a function of probe displacement and the measured ones in the case of the sample with crack 5. We notice that the two results are generally in good agreement. [Touil 22a]

3.3. CONCLUSION

In this chapter, we discuss the practical aspect of this project, which consists of the conception, and construction of GMR probes sample and differential GMR probes, and the prototype with the different boards (the power board, the multiplexing, and the pre-amplification board) to make the system autonomous. A prototype unit is built and tested to demonstrate the proof of concept. We present all the experimental results during the practical tests of the GMR probe. These results in an acceptable concordance between the results of the measurements and those of the calculation.

Experimentally, we justifier the choice of the excitation coil by comparing two symmetrical coils, one of them with ferrite core T6 in the same conditions of experience (the same current passed from them); ferrite core T6 adds 78.16 % to the sensitivity of the differential GMR sensor. We demonstrated that the magnetic field generated by the excitation ferrite coil in the linear range of the transfer characteristic of the GMR sensor AAH002 02 used (0.6 Oe -3Oe), otherwise the magnetic field generated by the excitation coil without ferrite out of the linear range of GMR sensor.

CHAPTER 4
GMR probe application : Data inversion

Contents

4.1. Introduction

The objective of this chapter is the application of the GMR probe built in chapter 3 in an eddy current control device in order to estimate the length and the depth of a defect. For this, we propose an inversion of the signals coming from the response of the NDT-EC differential GMR probe using the neural network (NN) method to reconstruct the length and depth of the defect and obtain its geometric characterization by solving the inverse problem.

In this context, a 3D finite element simulation is used to create a database that comprises the tension of the GMR probe-crack part system (constituting the crack signature) and is validated by an experimental companion. MATLAB software are implemented these different Neural network (NN) methods for solving the inverse problem.

4.2. Inverse Problem

The objective is to estimate the characteristic quantities of the material not accessible by direct measurement. For this, we have only information from the acquisition of EC sensors. That is what is known as an inverse problem because we determine these parameters by indirect measurement. To get back the quantities of interest from the observed quantities (different acquisitions from EC sensor)

4.3. Neural networks

A neural network (NN) is a synthetic network base on a simplified biological neuron model. Which is a nerve cell's essential element of the central nervous system. It is composed of critical parts represented in Figure 4.1.

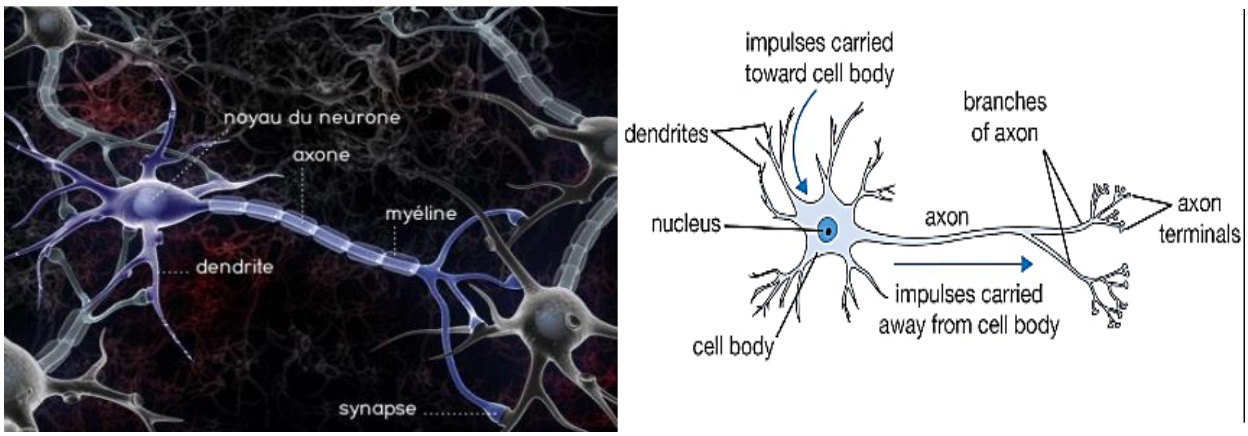

Fig 4.1 Diagram of a biological neuron [Réseaux 16, Intelligence 16, Artificial 18] at the level of the synapses, the transmission of information is done by chemical intermediaries: the neuromodulators.

The NNs in this work result from an attempt at mathematical modeling of the human brain. The first works date from 1943 and are the work of MacCulloch and Pitts [Baghli 99]. They invented the first formal neuron. They believe that the nervous impulse is the result of a simple calculation carried out by each neuron and that neuron and that thought arises through the collective effect of a network of interconnected neurons.

Each formal neuron is an elementary processor. It receives a variable number of inputs from upstream neurons. Each of these inputs is associated with a weighted representative of the strength of the connection. Each elementary processor has a single output, which then branches out to feed a variable number of downstream neurons. Each connection is associated with a weight (see figure.4.2).

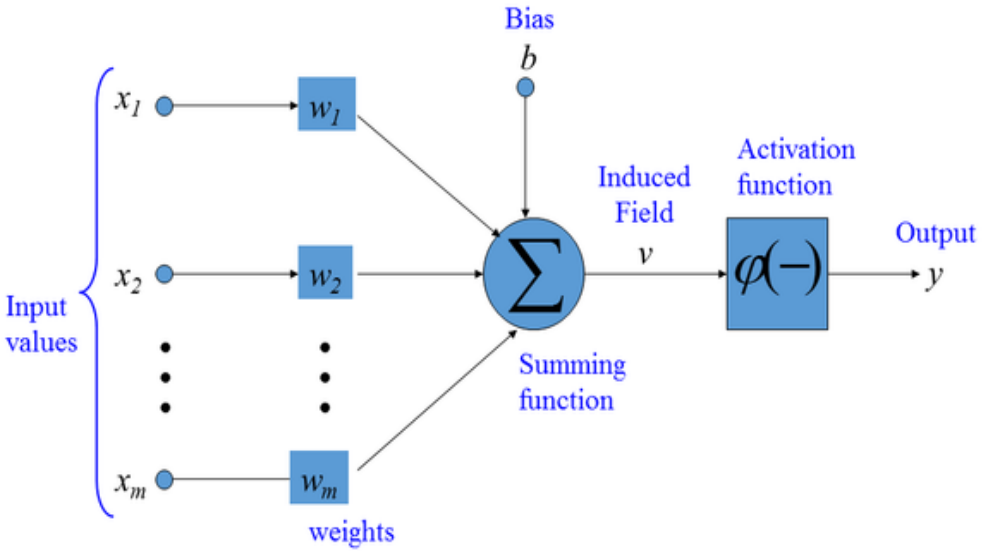

Fig 4.2 The artificial neuron Model [Intelligence 16]

From the above description, the output of the neuron is given by:

$$y = f_{\alpha}\left(\sum_{1}^{n} w_i x_i + b_0\right)$$

A neuron's behavior describes by the value of its connections (weights and biases) and activation function. The choice of the activation function is of great importance. It depends on the application to study [Hulusi 08].

4.3.1. Activation functions

The activation function defines the output potential of a neuron in terms of the activity levels of its inputs; there; there are several activation functions present in table 4.1 below:

Table 4.1 Activation functions

Asymmetric threshold function (hard limit)	$f(X) = \begin{cases} 1 & Si\ X > \beta \\ 0 & Si\ X \leq \beta \end{cases}$	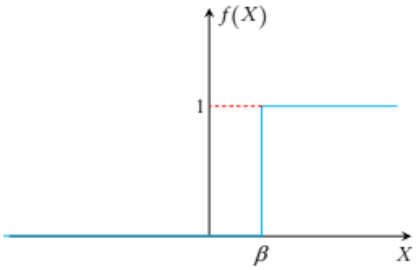
Sigmoid function b : Gain of the activation function	$f(X) = \frac{1}{1 + e^{-bX}}$	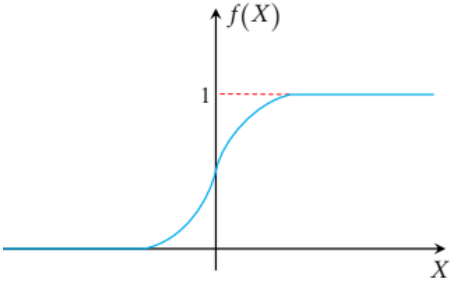
Saturation function	$f(X) = \begin{cases} 1 & Si\ X > \beta \\ X & Si\ -\beta < X < \beta \\ -1 & Si\ -\beta < X \end{cases}$	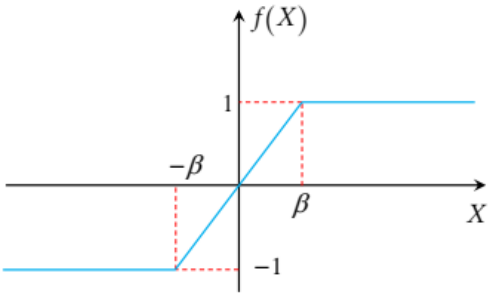
Centered Gaussian function σ: The standard deviation of the gaussian.	$f(X) = \exp(-\frac{1}{2}\frac{X^2}{\sigma^2})$	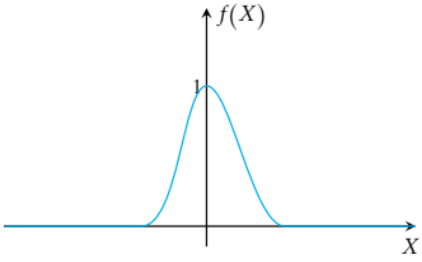

The activation function can be linear or non-linear. Among the different activation functions [Chady 00, Lebihan 00, Helifa 16b], selected according to the problem to solve, the Sigmoid functions are the most frequent [Oussar 98].

4.3.2. The modeling of non-linear problems by NN

The behavioral laws of EC sensors are highly nonlinear. Therefore, the adopted models must be nonlinear. There are NN structures capable of modeling these types of problems. Among these structures. The MLP (Multi-Layer Perceptron) neural networks are the most important and widely used [Chady 00, Lebihan 00]

4.3.3. Neural network Composition

A neuron realizes a non-linear function of its inputs. However, a single neuron is insufficient in most applications, and associating several neurons together is necessary. The association of several neurons in a network allows the composition of the non-linear functions realized by each neuron, which is particularly desirable for modeled systems whose behavior is not simple.

This combination of neural cells calls an artificial neural network, the structure geometry and learning methods study in the following sections.

An artificial neural network generally consists of three layers (see figure 4.3):

Input layer: It consists of all the neurons of the network that receive the data of the problem. Its size determines directly by the number of input variables.

Output layer: It consists of all the output neurons of the network. This layer provides the results of the problem.

Hidden layers are between the input layer, the input layer, and the output layer. They define the internal activity of the network. In general, these layers' activation functions are non-linear [Oukacine 12].

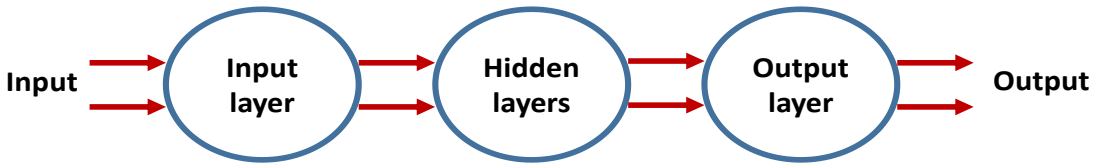

Fig 4.3 Neural network architecture

4.3.4. Neural network architecture

There are mainly two categories of NN: feed-forward and recurrent neural networks. The feed-forward is represented by a set of neurons connected whose information flows from the input to the output without going backward (Figure 4.4a). The output of this type of network does not

depend on time. The direction of the arrows in Figure 4.4 indicates the information's travel direction. In recurrent NN, the data in recurrent NN, information can also flow from one neuron to the one before (Figure 4.4b). Thus, the output of a neuron can also depend on itself. The choice of one or the other two types of NN depends on the application is treated [Hulusi 08].

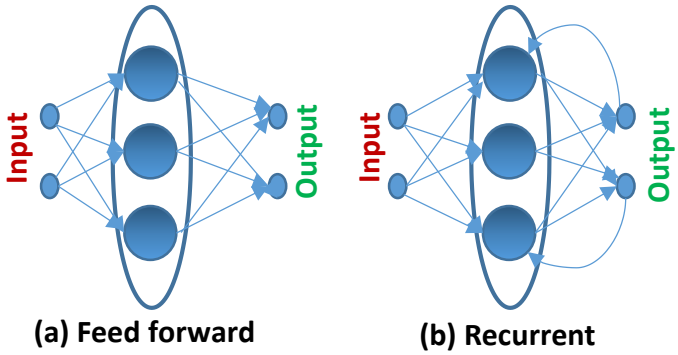

Fig 4.4 Examples of NN

In this dissertation work, we are interested in non-looped NN. Looped NN is typically used to perform time-dependent modeling tasks of dynamic systems (see figure 4.5).

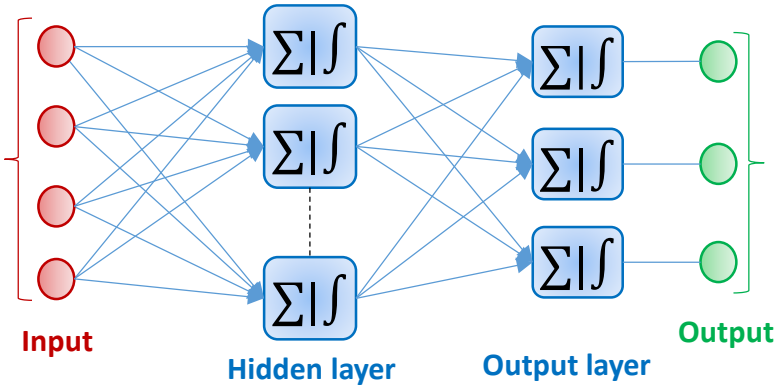

Fig 4.5 Structure d'un NN MLP

4.4. Neural networks Learning

An NN is characterized by the function defining each neuron and by the topology of the network. In general, the complete description of an NN also requires specifying the algorithm used for its learning. Thus, it is necessary to define a cost function measuring the difference between the output of the network and the desired solution and an algorithm for minimizing the cost function concerning the parameters. Often the mean square error (MSE) function is used as a cost function. Let W be a column vector consisting of all the weights and biases of the network. Noting

S, the function realized by the R and N, the number of examples, defines the MSE by the following relation:

$$MSE = \frac{1}{N}\sum_{K=1}^{N}(t(k)-\alpha(k))^2$$

Where N is the number of examples in the learning database, t (k) denotes the target vector, and a (k) denotes the network's developed output vector, MSE stands for the average quadratically erroneous output.

Among the most used learning algorithms, we can mention the Levenberg-Marquardt "Back-propagation" gradient algorithm, generally used for multilayer networks. This algorithm reuses the different steps of gradient computation, from the output layer to the inner layers, thus minimizing the number of calculations performed [Bensetti 04, Smid 05].

4.5. Characterization of open cracks: Implementation of inversion methods

We are interested in implementing inversion methods to estimate the physical or geometric parameters of the parts that are controlled (Figure 4.6). The response of the differential GMR probe constitutes database is simulated using a finite element numerical model defined in chapter 2. The studied application consists of the implementation of inverse models that simultaneously estimate the two important parameters of the crack, depth and length. In this application, a neural model is processed.

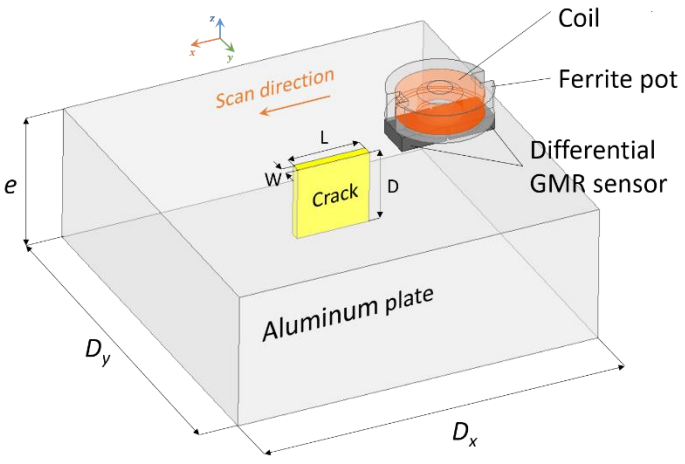

Fig 4.6. Dimensions of the test sample and probe geometry.

Figures 4.7 show the eddy current signals, i.e., the tension variations of the differential GMR probe simulated on the aluminum plate containing ten straight slots of different geometric

parameters (length and depth); the slots are perpendicular to the sample's surface. These signals constitute the simulation signature of the flaws.

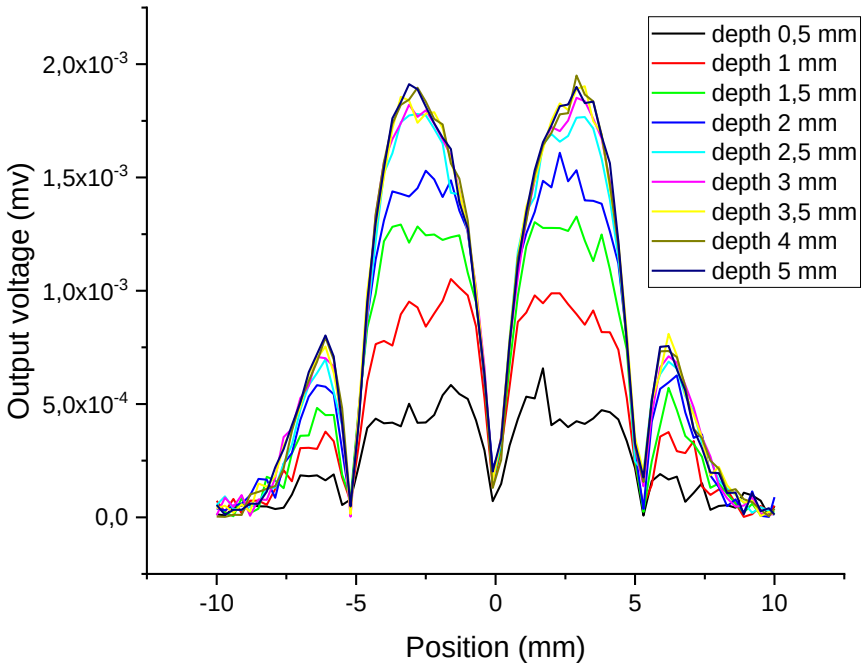

Fig 4.7 Tension variations as a function of the probe position for different crack depth value

4.6. Validation of 3D FE model

In Chapter 3, we validated the 3D FE model by experimental measurements using a standard with parallelepiped defects having different length and depth made by electric discharge machine as shown in Figure 4.8.

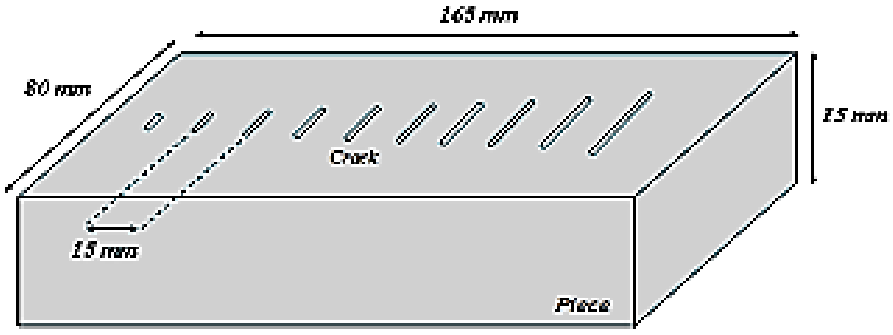

Fig 4.8 Cracks in different dimensions

Table 4.2 Dimensional data of cracks

Cracks	Length (mm)	Depth (mm)
1	1	1
2	2	2
3	3	3
4	4	4
5	5	5
6	6	5
7	7	5
8	8	5
9	9	5
10	10	5

4.6.1. Creating of Database

The inversion consists in going back from the sensor response to the parameters (depth, length). For the NN, as shown in the schematization in figure 4.9. The input of the NN consists of the sensor voltage (vector constituting the signature of the crack), and the output is the estimated crack depth and length.

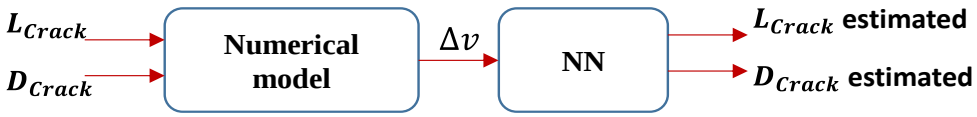

Fig 4.9 Inversion with NN

The physical problem is governed by a nonlinear system hence the choice of a nonlinear multilayer network, the structure for this application consists of a hidden layer with a hyperbolic tangent activation function and an output layer with a linear activation function. There is no general method to fix a network architecture (number of neurons in the hidden layer) for a given problem of neurons in the hidden layer) for a given situation, In this context, we are led to study a certain number of neural architectures (figure 4.10).

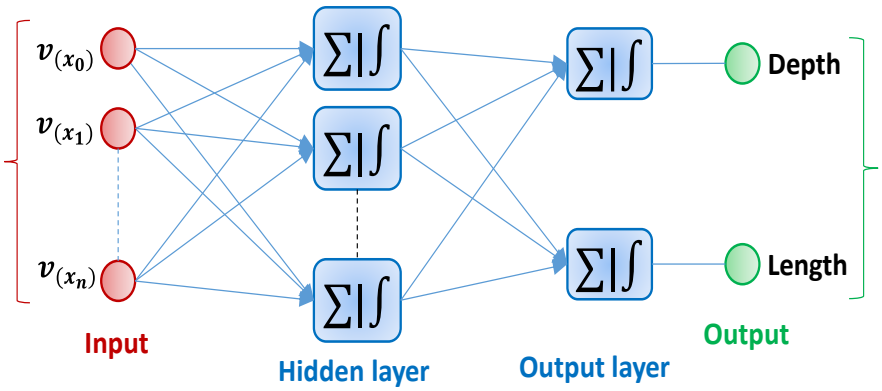

Fig 4.10 MLP Network Implementation

Perceptron multi-layers for the crack characterization comprise 63 neurons in the hidden layer with a hyperbolic tangent activation function and two output neurons with a linear activation function. The network receives the tension variation values as its input and supplies the crack parameter values (length and depth) as its output, as shown in Figure 4.10. The learning is done using the Levenberg Marquardt algorithm.

Figure 4.11 shows that after more than nine passes of the learning base, the algorithm converges toward the minimum tolerated error while adjusting the weights and biases values of the network. When the weights and the biases are adapted, we recover the values of the estimated crack parameters at the network output. The network learning results show a good correlation between the real and estimated outputs as shown in Figure 4.11 and Figure 4.12.

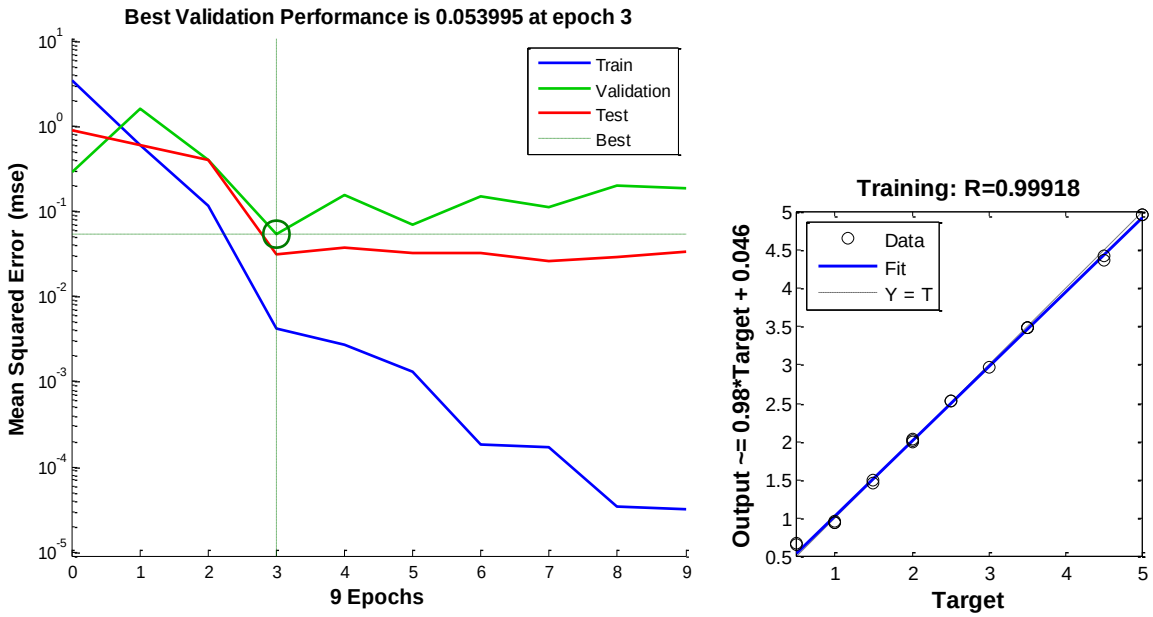

Fig 4.11 MSE on learning base, the correlation between the desired output and the network output for crack Depths.

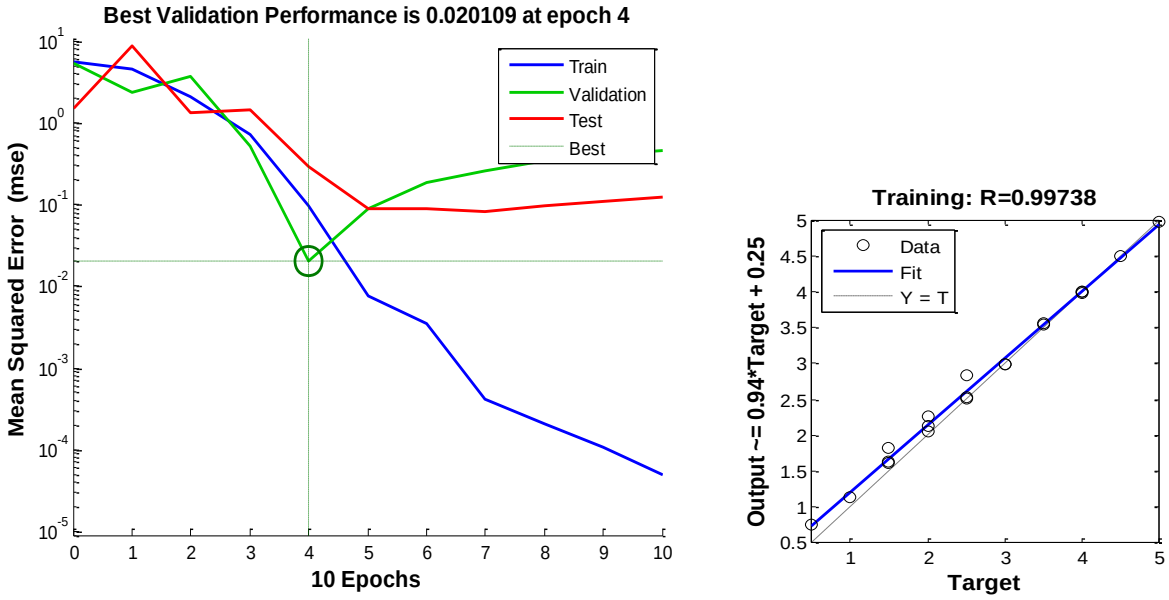

Fig 4.12 MSE on learning base, the correlation between the desired output and the network output for crack Length.

4.7. **Validation of results**

In this phase, the network capacity tests determine the target parameters (lengths and depths) corresponding to the examples of tension in the learning area.

We fed the network with an unlabeled input vector from the validation base, and the neural network calculated the output vector, the results shown in figures 4.13 (depth) and Figure 4.14(length), where the MSE are 0.053 and 0.0201 for depths and lengths; the neuron network learning results show a good correlation. This method requires good preparation of the learning base, which significantly influences the obtained results.

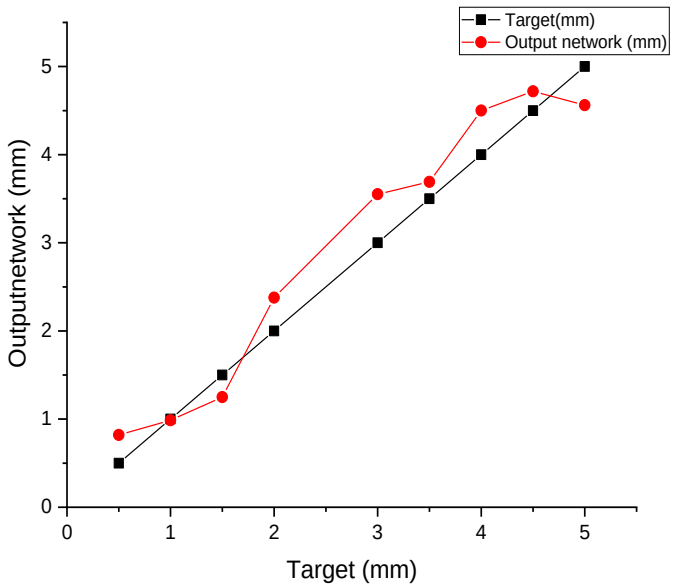

Fig 4.13 Depth of crack evaluated by ANN (Output) versus real value of crack and depth of specimen (Target)

The error between the real and estimated parameters is characterized for each parameter (P) by the relative error defined by the following relation:

$$ER(P) = \sqrt{\frac{1}{N}\sum_{i=1}^{N}\left(\frac{\hat{P}_i - P_i}{P_i}\right)}$$

With N, $\hat{P}_i$, and P_i, representing respectively, the number of examples on the test base, the real parameters, and the parameters estimated by the NN. The error commits for the estimation of the Length shown in Figure 4.14a, Following the results obtain we remark that the error is infinitesimal.

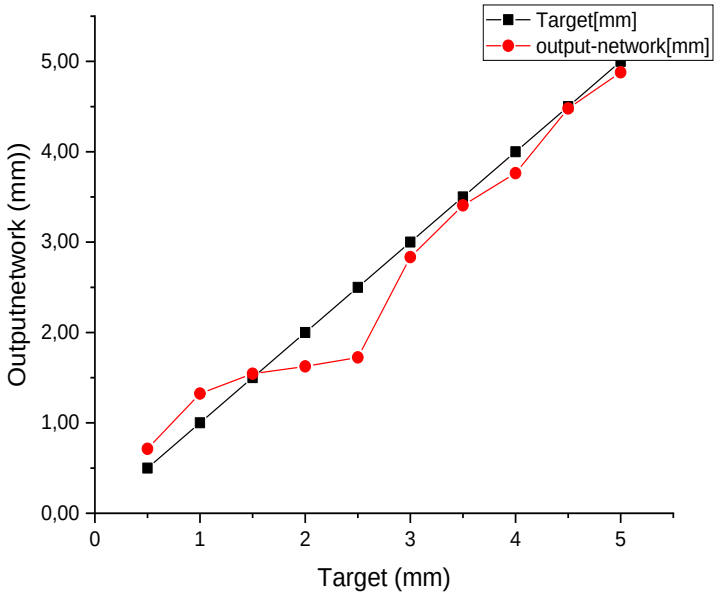

Fig 4.14 Length of crack evaluated by ANN (Output) versus real value of crack and depth of specimen (Target)

4.8. Conclusion

The contribution of the last chapter comes down to the inversion of data from the EC-NDT differential GMR probe for the detection and sizing of the various defects of conductive materials by the NN method and validated by experimental measurements. The results can be summarized as follows:

- The configuration of the magnetic probe (differential GMR probe) for an application to the deduction of the morphology of the crack is carried out.
- A database by solving the direct 3D finite element problem is built for data inversion by artificial neural networks.
- The integration of the GMR probe in an experimental measurement bench is carried out.
- Experimental measurements of voltage and data storage are carried out.
- The EC differential GMR probe signature depends on the crack length and depth, which are crucial parameters for thin cracks.
- Validation of the numerical model is made using voltage measurements from experimental measurements.
- This method requires good preparation of the learning base, which considerably influences the results obtained.

General conclusion and perspectives

GENERAL CONCLUSION

The aim of this thesis is to develop the strategy of elaborating software and hardware tools for the design and construction of new high-sensitivity magnetic sensors (GMR probe), using two symmetrical GMR sensors measuring the output voltage, in eddy current non-destructive testing in its experimental and simulation aspects, for the characterization of cracks in "critical" parts of conducting materials.

Two probes, simple and differential GMR probes, are realized during this thesis. An Approach's originality uses two symmetrical Giant magnetoresistance sensors in a differential configuration using commercial GMR elements inserted on a coil in a ferrite pot. The giant magnetoresistance (GMR) based eddy currents probe is more sensitive than the inductive probe. The GMR-based EC probe with a ferrite pot core is more sensitive to the presence of cracks than the conventional EC sensor without a ferrite pot core. The background signal measured by the sensor is tiny if there is no crack in the sample. The designed sensor demonstrates a high sensitivity to defects where the GMRs mounted in differential allow for reducing the impact of the background voltage.
These results can be summarized as follows :

- The 3-D model uses to compute the magnetic field strength of the permanent magnet to evaluate detectable area dimensions of the GMR AAH002 02 sensor, an experimental prototype unit consisting of the GMR sensor proposed and the permanent magnet as a distance function (Axial Magnet), and microcontroller interface. The magnetic field B change the output voltage on the GMR sensor. The inverse problem goal function is minimized using the particle swarm optimization (PSO) algorithm to evaluate the detectable area dimensions according to the measurement of the magnetic field strength at the GMR sensor's location.

- The notion of the GMR sensor's effective area (EA) using the 3-D numerical model to adjust the position of the GMR sensors-excitation coil at the optimal sensitivity point of the probe is found to be about 2.67mm from the center of the excitation coil.

- The comparison between the 3-D computed magnetic field strength of the permanent magnet and the measured one show a significant concordance. The maximum error between the two results is less than 2%.

We discuss the practical aspect of this project, which consists of the conception, and construction of GMR probes sample and differential GMR probes, and the prototype with the different boards (the power board, the multiplexing, and the pre-amplification board) to make the system autonomous. A prototype unit is built and tested to demonstrate the proof of concept. We present all the experimental results during the practical tests of the GMR probe. These results in an acceptable concordance between the results of the measurements and those of the calculation.

Experimentally, we justifier the choice of the excitation coil by comparing two symmetrical coils, one of them with ferrite core T6 in the same conditions of experience (the same current passed from them); ferrite core T6 adds 78.16 % to the sensitivity of the differential GMR sensor. We demonstrated that the magnetic field generated by the excitation ferrite coil in the linear range of the transfer characteristic of the GMR sensor AAH002 02 used (0.6 Oe -3Oe), otherwise the magnetic field generated by the excitation coil without ferrite out of the linear range of GMR sensor.

The contribution of the last chapter comes down to the inversion of data from the EC-NDT differential GMR probe for the detection and sizing of the various defects of conductive materials by the NN method and validated by experimental measurements. The results can be summarized as follows:

- The configuration of the magnetic probe (differential GMR probe) for an application to the deduction of the morphology of the crack is carried out.
- A database by solving the direct 3D finite element problem is built for data inversion by artificial neural networks.
- The integration of the GMR probe in an experimental measurement bench is carried out.
- Experimental measurements of voltage and data storage are carried out.
- The EC differential GMR probe signature depends on the crack length and depth, which are crucial parameters for thin cracks.
- Validation of the numerical model is made using voltage measurements from experimental measurements.
- This method requires good preparation of the learning base, which considerably influences the results obtained.

This device has typical characteristics required in NDT magnetic applications, especially in manufacturing electromagnetic units. This sensor is easy to manufacture industrially, according to its high characterization, which makes it very attractive and reliable.

PERSPECTIVES

Looking ahead, we propose the following improvements:

- Improvement and generalization of the sensor realized to take into account the different geometries and characteristics of the composites;
- Sensor hybridization made with GMR, AMR, and TMR magnetic sensors to increase the detection capabilities of defects in complex materials (CFCs);
- Improving the performance of neural networks by enriching its database to identify several physical parameters of composite materials with the minimum of errors;

Scientifique contribution

INTERNATIONAL JOURNAL PUBLICATIONS

- Dalal Radia Touil, Ahmed Chaouki Lahrech, Bachir Helifa, and Ibn Khaldoun Lefkaier, "Simulation and Implementation of a High Sensitive Differential Eddy Current Giant Magnetoresistance Probe for Non-Destructive Testing", *ISSN 1061-8309, Russian Journal of Nondestructive Testing, 2022, Vol. 58, No. 9, pp. 833–846. © Pleiades Publishing, Ltd., 2022.*
  ***DOI:** 10.1134/S1061830922090029*
- TOUIL Dalal Radia, DAAS, Ahmed, HELIFA, Bachir, and Ibn Khaldoun Lefkaier. Simple Giant Magnetoresistance Probe Based Eddy Current System of Defect Characterization for Non-Destructive Testing. Advanced Electromagnetics, 2022, vol. 11, no 2, p. 43-48.
  ***DOI:** 10.7716/aem.v11i2.1910*
- DALAL RADIA, Touil, AHMED, Daas, BACHIR, Helifa, and Ibn Khaldoun Lefkaier. Detection of Defects Using GMR and Inductive Probes. In : *International Conference in Artificial Intelligence in Renewable Energetic Systems*. Springer, Cham, 2019. p. 617-622.(Book chapter).
  ***DOI:** 10.1007/978-3-030-37207-1_66.*

NATIONAL PUBLICATION

- TOUIL Dalal Radia, LAHRECH Ahmed Chaouki, BARRARAT Fatima, HELIFA Bachir, LEFKAIER Ibn Khaldoun, DAAS Ahmed Modelling, "Eddy current GMR sensor characterization of surface cracks in an aluminum alloy" *Design and Optimization of Electromagnetic and Induction Devices Selected papers from Inductics Conference 2022 Coordinated by Mouloud FELIACHI.* . (Book chapter). © EPBI Editor 2022.

INTERNATIONAL CONFERENCES

- Touil Dalal Radia, Daas Ahmed, Helifa Bachir , Ibn Khaldoun Lefkaier 'Detection of Defects Using GMR and Inductive Probe '3rd International conference on Artificial intelligence in renewable energetic system IC-AIRE2019. Novembre 26-28,2019, Taghit Bachar, Algeria.

NATIONAL CONFERENCES

- TOUIL Dalal Radia, Daas Ahmed, Helifa Bachir, Ibn Khaldoun Lefkaier,"Characterization of crakcks by Eddy Current inductive and GMR Probes''. *Conférence national on physique Applique CPA19*, Octobre 03-04 2019, Laghouat, Algérie.
- TOUIL Dalal Radia, Daas Ahmed, Helifa Bachir , Ibn Khaldoun Lefkaier, "comparison of eddy current inductive and GMR Probes", *6th Colloque on inductique*. Octobre 28-29 2019, Biskra, Algeria.
- TOUIL Dalal Radia, Helifa Bachir, Ibn Khaldoun Lefkaier, Daas Ahmed, Caractérisation par courants de Foucault des fissures surfaciques dans un alliage d'aluminium, *1rst Journée Doctorale en Sciences de la Matière,* 09 Décembre 2021, Laghouat, Algérie.
- TOUIL Dalal Radia, Lahrech Ahmed Chaouki, Fatima Barrarat, Helifa Bachir, Lefkaier Ibn Khaldoun ,Daas Ahmed," Caractérisation par capteur GMR à courants de Foucault des fissures surfaciques dans un alliage d'aluminium". *7ème colloque sur l'inductique CI'2021*. 10-11 Mai 2022, Constantine, Algérie.

Bibliographic references

BIBLIOGRAPHIC REFERENCES

[Abdelli 14] Abdelli, Djamel Eddine. Modélisation par les volumes finis d'un problème de contrôle non destructif de forme complexe. Diss. Université Mohamed Khider Biskra, 2014.

[Artificial 18] Artificial Neuron : https://www.gabormelli.com/RKB/Artificial_Neuron (Consulté le 2018-01-14).

[Baghli 99] L. Baghli. Contribution à la commande de la machine asynchrone, utilisation de la logique floue, des réseaux de neurones et des algorithmes génétiques. PhD thesis, Université Henri Poincaré-Nancy I, 1999.

[Baibich 88] Baibich, Mario Norberto, et al. "Giant magnetoresistance of (001) Fe/(001) Cr magnetic superlattices." Physical review letters 61.21 (1988): 2472.

[Belkhiri 03] Belkhiri, Yamina. Modélisation des phénomènes électromagnétiques et mécaniques couples par la méthode des volumes finis (CVM). Diss. Université de Batna 2, 2003.

[Bensetti 04] Mohamed Bensetti, Etude et modélisation de capteurs destinés au contrôle non destructif par courants de Foucault. Mise en œuvre de méthodes d'inversion, Thèse de doctorat, Université Paris-Sud XI, 2004.

[Bernieri 19] Bernieri, Andrea, et al. "Eddy current testing probe based on double-coil excitation and GMR sensor." IEEE Transactions on Instrumentation and measurement 68.5 (2019): 1533-1542.

[Bensetti 08] Bensetti, Mohamed, et al. "Adaptive mesh refinement and probe signal calculation in eddy current NDT by complementary formulations." IEEE transactions on magnetics 44.6 (2008): 1646-1649.

[Bour 96] Bour, J-C., et al. "Étude de la répartition des courants de Foucault pulsés dans une configuration de contrôle non destructif." Journal de Physique III 6.1 (1996) : 7-22.

[Bíró 99] Bíró, Oszkár. "Edge element formulations of eddy current problems." Computer methods in applied mechanics and engineering 169.3-4 (1999): 391-405.

[Biro 89] Biro, Oszkar, and Kurt Preis. "On the use of the magnetic vector potential in the finite-element analysis of three-dimensional eddy currents." IEEE Transactions on magnetics 25.4 (1989): 3145-3159.

[Bouchala 08] Bouchala, Tarek. Modélisation Semi-Analytique des Courants de Foucault.– Application au Contrôle Non Destructif par des Capteurs à Noyau de Ferrite. Diss. Université de Batna 2, 2008.

[Choua 09] Choua, Yahya. Application de la méthode des éléments finis pour la modélisation de configurations de contrôle non destructif par courants de Foucault. Diss. Université Paris Sud-Paris XI, 2009.

[Catalog 21] www.nve.com.Availableonline: https://www.nve.com/Downloads/catalog.pdf (accessed 04 January, 2021).

[Chady 00] Tomasz Chady, Masato Enokizono, Ryszard Sikora, Neural Network Models of Eddy Current Multi-Frequency System for Nondestructive Testing, IEEE Transactions On Magnetics, Vol. 36, No. 4, July 2000, pp. 1724-1727

[Delabre 16] Delabre, Benjamin. Développement de capteurs flexibles à courants de Foucault: applications à la caractérisation des propriétés électromagnétiques des matériaux et à la détection de défauts par imagerie statique. Diss. Université Paris Saclay (COmUE), 2016.

[Doirat 07] Doirat, Vincent. Contribution à la modélisation de systèmes de Contrôles Non Destructifs par Courants de Foucault. Application à la caractérisation physique et dimensionnelle de matériaux de l'aéronautique. Diss. Université de Nantes, 2007.

[Dogaru 01] Dogaru, Teodor, and Stuart T. Smith. "Giant magnetoresistance-based eddy-current sensor." IEEE Transactions on magnetics 37.5 (2001): 3831-3838.

[Gao 18] Gao, Peng, et al. "Eddy current testing for weld defects with different directions of excitation field of rectangular coil." 2018 4th International Conference on Control, Automation and Robotics (ICCAR). IEEE, 2018.

[Gardiol 02] Gardiol, Fred. Electromagnétisme. Vol. 3. PPUR presses polytechniques, 2002.

[Hamia 12] Hamia, Rimond, Christophe Cordier, and Christophe Dolabdjian. "Separability of multiple deep crack defects with an NDE eddy current system." IEEE transactions on magnetics 49.1 (2012): 124-127.

[Hamia 10] Hamia, Rimond, et al. "Eddy current non destructive testing using an improved giant magnetoresistance magnetometer and a single wire as

inducer: a FEM performance analysis." IEEE Transactions on Magnetics 46.10 (2010): 3731-3737.

[Helifa 16b] Helifa, B., et al. "Characterization of surface cracks using eddy current NDT simulation by 3D-FEM and inversion by neural network." The Applied Computational Electromagnetics Society Journal (ACES) (2016): 187-194.

[Helifa 12] Helifa, Bachir. Contribution à la Simulation du CND par Courants de Foucault en vue de la Caractérisation des Fissures Débouchantes. Diss. Nantes, 2012.

[Helifa 16a] Helifa, B., et al. "Detection and measurement of surface cracks in ferromagnetic materials using eddy current testing." Ndt & E International 39.5 (2006): 384-390.

[Hulusi 08] Acikgoz, Hulusi. Technique d'inversion associant la modélisation numérique et les réseaux de neurones pour la caractérisation micro-ondes de matériaux. Diss. Paris 6, 2008.

[Intelligence 16] Intelligence artificielle :http://intelligence-artificielle-robotique.weebly.com (Consulté le 22 Février 2016).

[Iorio 07] Di Iorio, Federica. "Low field magnetic sensing with giant magneto resistive sensors." (2007).

[Jander 05] Jander, Albrecht, Carl Smith, and Robert Schneider. "Magnetoresistive sensors for nondestructive evaluation." Advanced Sensor Technologies for Nondestructive Evaluation and Structural Health Monitoring 5770 (2005): 1-13.

[Kuczmann 09] Kuczmann, Miklós. "Potential formulations in magnetics applying the finite element method." Lecture notes, Laboratory of Electromagnetic Fields,"Széchenyi István" University, Gyor, Hungary (2009).

[Lakhdar 11] Lakhdar, Ala-Eddine. "Etude et modelisation de capteurs en cnd par courants de foucault : application a la detection des fissures". Diss. Université Mohamed Khider-Biskra, 2011.

[Lebihan 00] Yann Lebihan, Conception et caractérisation d'un dispositif à courants de Foucault pour l'évaluation non destructive de l'épaisseur de paroi d'aubes de turbines creuses, Thèse de doctorat, Ecole Normale supérieure de Cachan, 2000.

[Lenz 06] Lenz, James, and S. Edelstein. "Magnetic sensors and their applications." IEEE Sensors journal 6.3 (2006) : 631-649.

[Moulder 92] Moulder, John C., Erol Uzal, and James H. Rose. "Thickness and conductivity of metallic layers from eddy current measurements." Review of scientific instruments 63.6 1992: 3455-3465.

[Oukacine 12] Oukacine, Nacima. Utilisation des réseaux de neurones pour la reconstitution de défauts en évaluation non destructive. Diss. Université Mouloud Mammeri, 2012.

[Oussar 98] Yacine Oussar, Réseaux d'ondelettes et réseaux de neurones pour la modélisation statique et dynamique de processus, Thèse de doctorat, Université Pierre et Marie Curie Paris 6, France, 1998.

[Postolache 10] Postolache Octavian, H. Geirinhas Ramos, and A. Lopes Ribeiro. "Detection and characterization of defects using GMR probes and artificial neural networks." Computer Standards & Interfaces 33.2 (2011): 191-200.

[Ramirez 10] Ramirez-Pacheco, E., et al. "Defect detection in aluminium with an eddy currents sensor." 2010 IEEE Electronics, Robotics and Automotive Mechanics Conference. IEEE, 2010.

[Réseaux 16] Réseaux de neurones : http://www.pinville.com/reseaux-de-neurones.php (Consulté le 22 Février 2016).

[Reig 13] Reig, Candid, Susana Cardoso, and Subhas Chandra Mukhopadhyay. "Giant magnetoresistance (GMR) sensors." Smart Sensors, Measurement and Instrumentation 6.1 (2013): 1-301.

[Rifai 16] Rifai, Damhuji, et al. "Giant magnetoresistance sensors: A review on structures and non-destructive eddy current testing applications." Sensors 16.3 (2016): 298.

[Romero 20] Romero-Arismendi, N. O., et al. "Design method for a GMR-based eddy current sensor with optimal sensitivity." Sensors and Actuators A: Physical 314 (2020): 112348.

[Rubinacci 08] Rubinacci, Guglielmo, Antonello Tamburrino, and Salvatore Ventre. "An efficient numerical model for a magnetic core eddy-current probe." IEEE transactions on magnetics 44.6 (2008): 1306-1309.

[Santandréa 10] Santandréa, Laurent, and Yann Le Bihan. "Using COMSOL-multiphysics in an eddy current non-destructive testing context." Proceedings of the COMSOL Conference. Vol. 44. 2010.

[Smid 05] Radislav Smid, Adam Docekal, Marcel Kreidl, Automated classification of eddy current signatures during manual inspection, NDT&E International, Elsevier, Vol. 38, February 2005, pp.462-470.

[Smith 04] Smith, C. H., et al. "Eddy-Current Testing with GMR Magnetic Sensor Arrays." AIP Conference Proceedings. Vol. 700. No. 1. American Institute of Physics, 2004.

[Smith 99] Smith, Carl H., and Robert W. Schneider. "Low-field magnetic sensing with GMR sensors." Sensors EXPO. 1999. pp 1-13.

[Thollon 95] Thollon Frédéric, Conception et optimisation de capteurs à courants de Foucault pour la détection de défauts profonds dans des matériaux amagnétiques, Thèse de doctorat, Ecole centrale de Lyon, 1995.

[Touil 22a] Touil D R, Lahrech A C, Helifa B, and Lefkaier I K, "Simulation and Implementation of a High Sensitive Differential Eddy Current Giant Magnetoresistance Probe for Non-Destructive Testing", ISSN 1061-8309, Russian Journal of Nondestructive Testing, 2022, Vol. 58, No. 9, pp. 833–846. © Pleiades Publishing, Ltd., 2022. DOI: 10.1134/S1061830922090029

[Touil 22b] Touil, Dalal Radia, et al. "Simple Giant Magnetoresistance Probe Based Eddy Current System of Defect Characterization for Non-Destructive Testing." Advanced Electromagnetics 11.2 (2022): 43-48.

[Touil 19] Dalal Radia, Touil, et al. "Detection of Defects Using GMR and Inductive Probes." International Conference in Artificial Intelligence in Renewable Energetic Systems. Springer, Cham, 2019.

[Vacher 07] Vacher, François. Développement d'un imageur magnétique pour le contrôle non destructif par courants de Foucault. Diss. Cachan, Ecole normale supérieure, 2007.

[Zaoui 08] Zaoui, Abdelhalim. Contribution à la modélisation du CND par matrice de capteurs à courants de Foucault. Diss. Nantes, 2008.

[Zemouri 16] Zemouri, Nassima. Etude et Réalisation d'un Système Multi-capteurs Destiné au Diagnostic des Matériaux Conducteurs. Diss. Université Mouloud Mammeri, 2016.

[Zerguini 09] Sakina, Zerguini. "Elaboration de modèles électromagnétiques caractérisant le contrôle non destructif par courant de Foucault."universite de constantine, constantine, Thèse de doctorat en science (2009).

[Zorni 12] Zorni, Chiara. "Contrôle non destructif par courants de Foucault de milieux ferromagnétiques : de l'expérience au modèle d'interaction". Diss. Université Paris Sud-Paris XI, 2012.

Abstract

Abstract: The aim of this thesis is to develop strategy of elaborating software and hardware tools for design and construction of high-sensitivity magnetic sensors (GMR probe) in eddy current non-destructive testing in its experimental and simulation aspects for the characterization of cracks in "critical" parts of conducting materials. In this context and to place the work in a more general framework. Two probes realize during this thesis simple and differential GMR probes. We propose a sample GMR probe and we show that the giant magnetoresistance (GMR) -based eddy currents probe is more sensitive than the inductive probe with a difference of 80 %. We propose a new design and implementation of a high-sensitivity eddy current (EC) sensor based on GMR to assess cracks in conductive materials. This approach's originality uses two symmetrical Giant magnetoresistance sensors in a differential configuration using commercial GMR elements inserted on a coil in a ferrite pot. The background signal measured by the sensor is infinitesimal if there is no crack in the sample. Therefore, the designed sensor demonstrates a high sensitivity to the presence of defects where the GMRs mounted in differential allow for reducing the background voltage's impact. On the other hand, The GMR-based EC probe with a ferrite pot core is more sensitive to the presence of cracks than the conventional EC sensor without a ferrite pot core. This work introduces the notion of the GMR sensor's effective area (EA) after being calculated and optimized using the inverse problem (Particle Swarm Optimization method). The operation of the differential GMR sensor is validated using a 3D Finite Element Model based on the (A, V–A) formulation and experimental measurements. Finally, the prototype of the differential GMR sensor is developed and tested. The experimental results are obtained to evaluate cracks machined on an aluminum standard. We validate (direct and reverse) by comparing the database comprising the tension of the GMR probe-crack (crack signature). We use the artificial neural network's method for the inversion of data in the NDT-EC differential GMR probe to detect and size the different defects in conductive materials while offering the advantages of high sensitivity and excellent reliability.
Keywords: Differential GMR probe, Simple probe, Non-destructive testing, Eddy currents, direct finite element model (FEM), inverse problem (PSO), cracks, artificial neural network's, Database.

Résumé : Le but de cette thèse est de développer une stratégie d'élaboration d'outils logiciels et matériels pour la conception et la construction de capteurs magnétiques à haute sensibilité (sonde GMR) dans les essais non destructifs par courants de Foucault dans ses aspects expérimentaux et de simulation pour la caractérisation des fissures dans les parties "critiques" des matériaux conducteurs. Dans ce contexte et afin de situer le travail dans un cadre plus général. Deux sondes réalisent au cours de cette thèse simple et différentielle sondes GMR. Nous proposons un exemple de sonde GMR et nous montrons que la sonde de courants de Foucault à base de magnétorésistance géante (GMR) est plus sensible que la sonde inductive avec une différence de 80 %. Nous proposons une nouvelle conception et mise en œuvre d'un CF à haute sensibilité Capteur basé sur GMR pour évaluer les fissures dans les matériaux conducteurs. L'originalité de cette approche utilise deux capteurs de magnétorésistance géants symétriques dans une configuration différentielle utilisant des éléments GMR commerciaux insérés sur une bobine dans un pot de ferrite. Le signal d'arrière-plan mesuré par le capteur est infinitésimal s'il n'y a pas de fissure dans l'échantillon. Par conséquent, le capteur conçu démontre une grande sensibilité à la présence de défauts lorsque les GMR montés en différentiel permettent de réduire l'impact de la tension de fond. En revanche, la sonde CF basée sur le GMR avec un noyau en pot de ferrite est plus sensible à la présence de fissures que le capteur CF classique sans noyau en pot de ferrite. Ce travail introduit la notion de zone efficace (ZE) du capteur GMR après avoir été calculée et optimisée à l'aide du problème inverse (PSO). Le fonctionnement du capteur différentiel GMR est validé à l'aide d'un modèle d'éléments finis 3D basé sur la formulation A, V–A et des mesures expérimentales. Enfin, le prototype du capteur différentiel GMR est développé et testé. Les résultats expérimentaux sont obtenus pour évaluer les fissures usinées selon une norme d'aluminium. Nous validons (direct et inverse) en comparant la base de données comprenant la tension de la sonde GMR-fissure (signature de fissure). Nous utilisons la méthode du réseau neuronal artificiel pour l'inversion des données dans la sonde GMR différentielle NDT-EC afin de détecter et de dimensionner les différents défauts dans les matériaux conducteurs tout en offrant les avantages d'une grande sensibilité et d'une excellente fiabilité.
Mots-clés : Sonde GMR différentielle, Sonde simple, control non destructif, Courants de Foucault, modèle direct d'éléments finis (FEM), problème inverse (PSO), fissures, réseau de neurones artificiel, Base de données.

الملخص: الهدف من هذه الأطروحة هو تطوير استراتيجية تطوير أدوات البرمجيات والأجهزة لتصميم وبناء مستشعرات مغناطيسية عالية الحساسية (مسبار لمقاومة المغناطيسية العظمى) في الاختبار غير المدمر لتيارات فوكو في الجانب التجريبي والمحاكاة لتوصيف الشقوق في أجزاء "الحرجة" من المواد الناقلة. في هذا السياق ولوضع العمل في إطار أكثر عمومية. تم تحقيق مجسين خلال هذه الأطروحة: مسبارين مسبار بسيط ومسبار المقاومة المغناطيسية العظمى التفاضلي. نقترح مسبار البسيط ونوضح أن مسبار تيارات فوكو القائمة على المقاومة المغناطيسية العملاقة أكثر حساسية من المسبار الحثي بفارق 80٪. نقترح تصميمًا جديدًا وانجازا لمسبار تيارات فوكو عالي الحساسية يعتمد على المقاومة المغناطيسية العظمى لتقييم العيوب في المواد الناقلة. هذه التقنية الحديثة تستخدم مستشعرين متماثلين للمقاومة المغناطيسية العملاقة في تصميم تفاضلي باستعمال عناصرها التجارية التي يتم وضعهما على الوشيعة في حامل من الفيرّيت. تكون إشارة جهد سطح العينة التي يقاسها المسبار متناهية الصغر إذا لم يكن هناك عيب في العينة. لذلك، يُظهر المسبار المصمم حساسية عالية لوجود العيوب حيث تسمح أنظمة للمقاومة المغناطيسية العملاقة التفاضلي بتقليل تأثير جهد سطح العينة. من ناحية أخرى، يكون مسبار تيارات فوكو المعتمد على المقاومة المغناطيسية العملاقة مع حامل الفيرّيت أكثر حساسية لوجود العيوب من مسبار تيارات فوكو العادي بدون حامل الفيرّيت. يقدم هذا العمل فكرة المساحة الفعالة (EA) لمستشعر المقاومة المغناطيسية العملاقة بعد حسابها وتحسينها باستخدام المشكلة العكسية (PSO). يتم التحقق من صحة مسبار المقاومة المغناطيسية العملاقة التفاضلي باستخدام نموذج العناصر المنتهية ثلاثية الأبعاد على أساس الصيغة *A*، *V-A* والقياسات التجريبية. أخيرًا، تم تطوير واختبار النموذج الأولي لمسبار المقاومة المغناطيسية العملاقة التفاضلي. يتم الحصول على النتائج التجريبية لتقييم الشقوق التي تم تشكيلها على معيار الألمنيوم. نحن نتحقق (مباشر وعكسي) من خلال مقارنة قاعدة البيانات التي تضم توتر مسبار المقاومة الاعظمية التفاضلي (اشارة العيب). نحن نستخدم طريقة الشبكة العصبية الاصطناعية لعكس البيانات لمسبار تيارات فوكو للفحص غير المتلف التفاضلي لاكتشاف وتحجيم العيوب المختلفة في المواد الناقلة مع تقديم مزايا الحساسية العالية والموثوقية الممتازة.
الكلمات المفتاحية:
مسبار المقاومة المغناطيسية العظمى التفاضلي، مسبار بسيط، الفحص الغير المتلف، تيارات فوكو، النمذجة بواسطة العناصر المنتهية ثلاثية الأبعاد، المشكلة العكسية، العيوب، الشبكات العصبية الاصطناعية، القاعدة البيانية.